Aalto University
School of Chemical
Technology

School of Chemical Technology
Degree Programme of Materials Science and Engineering

Asmo Pasanen

ONLINE CONTROL OF INCLUSIONS IN STEELMAKING

Master's thesis for the degree of Master of Science in Technology submitted for inspection, Espoo, 3.8.2015.

Supervisor Professor Seppo Louhenkilpi

Instructor M.Sc. Ari Kruskopf

Aalto University
School of Chemical
Technology

Aalto University, P.O. BOX 11000, 00076 AALTO
www.aalto.fi

Abstract of master's thesis

Author	Asmo Pasanen
Title of thesis	Online control of inclusions in steelmaking
Department	Materials Science and Engineering
Professorship	Metallurgy
Code of professorship	MT-37
Thesis supervisor	Professor Seppo Louhenkilpi
Thesis advisor(s) / Thesis examiner(s)	M.Sc. Ari Kruskopf
Date	3.8.2015
Number of pages	68
Language	English

Abstract

This work was done to FIMECC SIMP – project. Different models, methods and ideas for online model for online control of inclusions in steelmaking were investigated.

Ladle process is complex with many different phenomena affecting the system. Different phenomena of the ladle process were presented. The main phenomena are mixing, deoxidation, refractory wearing and vacuum degassing.

Three models from the literature were presented. Different models were discussed and conclusions and recommendations for future research were made. 'Tanks in series' model used by Shu & Scheller was proposed to be researched as a mixing module. The models by Harada et al. and Shu & Scheller were proposed to be researched more because of their refractory dissolution and inclusion modeling concepts. The 0-D model by Bellot et al. was proposed for offline research tool for estimation of size distribution of the inclusions.

Coupled reaction model for calculating the variations of steel/slag composition during ladle process was made and presented. Sensitivity analysis of this model was presented. It was concluded that the model is not sensitive to the range of values that were tested.

Keywords Inclusion, online, model, steelmaking

Aalto University
School of Chemical
Technology

Aalto University, P.O. BOX 11000, 00076 AALTO
www.aalto.fi

Abstract of master's thesis

Tekijä Asmo Pasanen		
Työn nimi Sulkeumien online -kontrollointi teräksen valmistuksessa		
Laitos Materiaalitekniikka		
Professuuri Metallurgia		**Professuurikoodi** MT-37
Työn valvoja Professori Seppo Louhenkilpi		
Työn ohjaaja(t)/Työn tarkastaja(t) DI Ari Kruskopf		
Päivämäärä 3.8.2015	**Sivumäärä** 68	**Kieli** Englanti

Tiivistelmä

Tämä työ tehtiin FIMECC SIMP – projektiin. Työssä tutkittiin eri malleja, metodeja ja ideoita online-malliin, jonka avulla voidaan kontrolloida sulkeumia teräksen valmistuksessa.

Senkkaprosessi on monimutkainen systeemi, johon vaikuttaa paljon eri ilmiöitä. Työssä esiteltiin näitä ilmiöitä, joista tärkeimmät ovat sekoittuminen, hapenpoisto, vuorauksen kuluminen ja kaasujen poisto.

Tässä työssä esiteltiin kirjallisuudesta kolme mallia. Malleja vertailtiin ja johtopäätöksiä sekä suosituksia tutkimuskohteiksi tehtiin. Sekoitusmoduuliksi suositellaan Shu & Scheller:n käyttämää ’Tanks in series’ –mallia. Harada et al.:n ja Shu & Scheller:n malleja suositellaan tutkimuskohteiksi heidän seinämien kulumisen ja sulkeumien mallintamiskonseptien johdosta. Sulkeumien kokojakauman offline –mallintamiseen suositellaan Bellot et al.:n 0-D –mallia.

Työssä tehtiin malli teräksen/kuonan koostumuksen vaihtelulle senkkaprosessissa. Mallin käyttäytymistä tutkittiin herkkyysanalyysilla. Malli ei ole sensitiivinen testatulle arvoalueelle.

Avainsanat Sulkeuma, malli, online, teräksen valmistus

Preface

I would like to thank my professor Seppo Louhenkilpi and my instructor Ari Kruskopf for all their help and patience. It has been a pleasure to work at laboratory of metallurgy.

Thanks to Dr. Shao Lei for his work and instructions.

Heaps of thanks to my lovely wife Elina for all the help and support.

Thanks heaps also to all my friends and family for the support.

Espoo 30.07.2015

Asmo Pasanen

Nomenclature

a_i	Activity of the element i	()
A	Area	(m^2)
B_i	Birth rate of class i	($1/m^3s$)
C	Total number of moles in the liquid slag phase	()
C_i	Surface capture contribution	($1/m^3s$)
$C_S^{'}$	Sulfur capacity	()
d	Diameter	(m)
d_b	Equivalent gas bubbles diameter	(m)
d_{pi}	Particle diameter representative of the class i	(m)
D	Diffusion coefficient	(m^2s)
D_i	Death rate of class i	($1/m^3s$)
E_c	Collision efficiency	()
E_i	Equilibrium partition ratio of element i	()
f_i	Activity coefficient of the element i by Raoult's law	()
$\boldsymbol{F}$	Interaction forces between gas and liquid phases	(N)
g	Gravitational acceleration	(m/s^2)
h	Depth	(m)
h_0	Injection depth	(m)
J	Molar flux density	(mol/m^2s)
k	Mass transfer coefficient	(m/s)
K	Equilibrium constant	()
l	Characteristic length	(m)
M	Molecular or atomic weight	(g/mol)
N_b	Numeral density of bubbles	($1/m^3$)
N_i	Number of inclusions of class i per m^3	($1/m^3$)
p	Pressure	(Pa)
P_a	Atmospheric pressure	(Pa)
Q	Argon gas flow rate	(Nm^3/min)
r_r	Refractory thickness	(m)
r_{mass}	Mass recirculation rate	(kg/s)
R	Gas constant	(J/molK)
Re	Reynolds number	[l*u/v]
S	Total molar concentration	(mol/m^3)
S_i	Inclusion gravity separation term	($1/m^3s$)
Sc	Schmidt number	[ν/D]
t	Time	(s)
t_m	Perfect mixing time	(s)
T	Temperature	(K)
u	Characteristic velocity	(m/s)
$\boldsymbol{u}$	Average velocity vector	(m/s)
$\boldsymbol{u_d}$	Adimensional inclusion deposition velocity	(m/s)
$\boldsymbol{u_s}$	Vertical Stokes velocity in the case of small inclusions	(m/s)
u_{slip}	Slip velocity between inclusion particle and the liquid steel phase	(m/s)

$\boldsymbol{u}^*$	Shear velocity of the liquid	(m/s)
U_{gl}	Average sliding liquid-bubble velocity	(m/s)
v	Circulation rate	(t/s)
w_i	Mass fraction of substance i	(%)
W	Weight	(t)
Z_{bi}	Flotation rate	(1/m^{3}s)
γ_i	Activity coefficient of the substance i	()
ΔG	Change of Gibbs free energy	(J/mol)
ΔG^0	Standard change of Gibbs free energy	(J/mol)
α	Retention rate	(m^3/m^3)
β_{bi}	Flotation frequency	(m^3/s)
β_{det}	Deterministic frequency	(m^3/s)
β_{ij}	Collision frequency between size classes i and j	(1/s)
$\beta_{turb,i}$	Stochastic frequency	(m^3/s)
$\dot{\varepsilon}$	Stirring energy	(W/t)
η	Fractional efficiency	()
κ	Volumetric mass transfer coefficient	(m^3/s)
μ	Dunamic Viscosity	(Pa*s)
ν	Kinematic viscosity	(m^2/s)
ρ	Density	(kg/m^3)
σ$_{m\text{-}s}$	Interfacial tension between liquid steel and slag	(N/m)
τ	Tensor of viscous stresses	()
$\boldsymbol{\tau_p^+}$	Dimensionless relaxation time of the inclusion	()
φ	Auxiliary variable	(1/s)
φ_i	Out-flow density of class i	(1/m^{2}s)
$(\,)^b$	Indicates the value in the bulk	
$(\,)^*$	Indicates the saturated concentration of substance i	
$(\,)^I$	Indicates the value in the interface	
$(\,)_k$	Index stands for each phase, liquid l and gas g	
$(\,)_s$	Value in the slag phase or value of the slag phase	
$(\,)_m$	Value in the liquid steel phase or value of the liquid steel phase	
$(\,)_M$	Value of element M	
$(\,)_I$	Value in the interface	
$(\,)_p$	Notation for inclusion	
$(\,)_r$	Notation for refractory	
$(\,)_v$	Value of the bath	

1. Introduction

The purpose of this work is to present ideas or guidelines for online model for better inclusion control in steel plants. Online model will promote quality of the steel by delivering information to the operator in real time. A few important properties of the online model are outlined here. Size, amount and composition of the inclusions in the liquid steel are being modeled. The model predicts the parameters of the inclusions and compares the values of modeled parameters to desired values. Differences in the modeled and desired values indicate the process has to be changed in order to reach the desired values of the steel. Online model should give suggestions to the operator to better operate the ladle process. Model could give for example following suggestions: “Too much dissolved oxygen in the liquid steel. Use more aluminium.” or “Inclusions are not removed from the liquid steel into the slag. Raise argon gas blowing to remove inclusion to the top slag.” Online model must be fast. This means that the total calculation time of the model must be small enough that changes to the process can be made based on the suggestions of the model. So the calculation time should be in maximum of seconds or few minutes rather than dozens of minutes. All the changes made to the ladle process should immediately give answers to the operator, how to better operate the process in order to be able to make steel with good quality. Model should be made to be fast without losing the accuracy of the model. This might not be possible but the best accuracy that can be achieved with limited amount of time is desired.

All the relevant phenomena in the ladle process should be modeled. Model consists of several modules which calculate the phenomena. Model should consider following things:

- The mixing of the liquid steel
- The mixing of the slag
- Reactions between inclusions and the liquid steel
- Reactions between inclusions and the slag
- Reactions between the liquid steel and the slag

- Reactions between the refractory lining and the liquid steel
- Reactions between the refractory lining and the slag

2. Basic phenomena and processes in the ladle

In 1950s steel started to be treated in the ladle. Secondary steelmaking has grown to be very important step of the steelmaking. The ladle processes have been improved in the years and many different processes have been developed and put in use. Operations in secondary metallurgy contains optimizing steel composition via deoxidation and desulfurization, homogenization and optimizing temperature of the steel for casting. Processes done in the ladle are deoxidation, desulfurisation, dephosphorisation, vacuum degassing (removal C, N, H, etc.), alloy addition, inclusion removal, modification of inclusion chemistry, homogenization of composition and temperature of the steel. Main objectives of ladle metallurgy are chemical composition and temperature control.

2.1. Tapping

Tapping of the steel starts the secondary metallurgy phase. Steel is tapped from converter or electric arc furnace (EAF) into ladle. During tapping air is entrapped into the stream of liquid steel and so nitrogen is entrapped into the liquid steel as notated in equation

$$N_2(g) \rightleftharpoons 2[N]. \qquad (1)$$

The higher the content of oxygen and/or sulfur in the liquid steel is the lower is the nitrogen pick up. This is because S and O are surface active elements. Tapping of the steel can also lead to slag carryover. Slag carryover from BOF or EAF (Electric arc furnace) is bad for secondary metallurgy because furnace slag contains a lot of FeO and MnO and is not suitable as refining slag in the refining phase of the steelmaking. Slag carryover can also lead to aluminium and silicon losses as well as phosphorous reversion. Aluminium and silicon reacts with less stable oxides, e.g., FeO and MnO and results in aluminium and silicon losses. Phosphorous reversion happens after

deoxidation of the steel and the amount of phosphor in the carryover slag and the amount of carryover slag defines the amount of phosphorous reversion. [1]

2.2. Slag

Slag has many important functions in the secondary steelmaking processes. Slag acts as thermal insulator therefore molten steel maintains temperature. Slag acts as a reaction barrier between molten steel and the atmosphere. Oxygen, nitrogen and hydrogen do not react with molten steel and reoxidation and pick-up of hydrogen and nitrogen are limited. Removal of inclusions from the molten steel gathers inclusions to the slag. Refining slag enables desulfurization, deoxidation and dephosporization. However slag reacts with refractory lining and wears it down. Basicity of the slag (%CaO/%SiO2) is important parameter to the success of desulfurization. [1]

2.3. Additions

Additions in the liquid steel can contain impurities and moisture. Nitrogen can be found in various ferroalloys and moisture on the additions adds hydrogen and oxygen pick up. Additions also affect the temperature of the steel which is called the chilling effect because usually temperature of the additions is low. The amount of temperature decrease due to additions correlates to the heat content of the additions. Some additions can also heat up the liquid steel due to chemical reactions between the addition and the bath. For example when aluminium reacts with the oxygen it is exothermic process. [1]

2.4. Ferroalloys dissolution/melting

Depending on the class of ferroalloys the dissolution/melting process is different. Class I ferroalloys have melting points lower and class II ferroalloys have melting points higher than the operating temperature of the liquid steel. When ferroalloys are added to the liquid steel solidified shell of steel solidifies on the surface of the additions because of local chilling effect. Then for class I ferroalloys solidified shell melts and the addition heats up to its melting point and the addition melts into the liquid steel. For

class I ferroalloys convective heat transfer as well as the size of the addition defines the melting speed. For class II ferroalloys solidified shell melts and addition heats up to the same temperature as the liquid steel. Dissolution of class II ferroalloys is the process which dissolves the addition into the liquid steel. This process is controlled by mass transfer and it is important that the size of the class II ferroalloys is kept between 3 – 10 mm. [1]

2.5. Refractory

The refractory material in the ladle affects the secondary steelmaking process via temperature losses and reactions between the refractory material and the liquid steel/slag/inclusions. Preheating of the ladle is important for minimizing refractory wear (useful service life). Too rapid heating of the hot face results in big temperature gradients in the ladle and therefore stresses the ladle, which wear the ladle faster than is reasonable. Preheating of the ladle also affects the temperature of the liquid steel as less heat is transferred into the ladle from the liquid steel. [2]

The refractory dissolves into the slag more than into the liquid steel. Slag and refractory forms a meniscus. Refractory dissolves oxides into slag at the meniscus which changes its surface tension. This results in Marangoni flow. Marangoni flow affects the steel so that the steel is pulled away from the refractory and the gap is closed with slag. Interfacial tension between slag and liquid steel is noted as $\sigma_{m\text{-}s}$ in Figure 1. Flow moves from lower interfacial tension areas to high interfacial tension areas, which results in gradual erosion of the refractory. This is illustrated in Figure 1. [2]

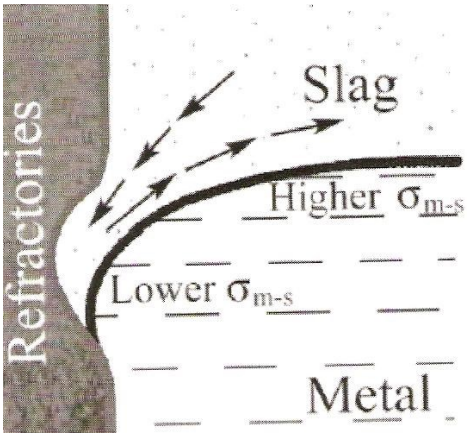

Figure 1. Erosion of refractory due to marangoni flow. [3]

The local corrosion of carbon-oxide refractory is illustrated in Figure 2. In Figure 2a slag due to marangoni flow will dissolve oxide part of the refractory into itself. After dissolving oxide from the refractory situation becomes non-wetting for slag and liquid steel will fill the gap. This is illustrated in Figure 2b. Then liquid steel dissolves the carbon containing part (graphite) of the refractory into itself. This process continues as a loop and accelerates the corrosion of refractory at the slag – liquid steel interface. [2]

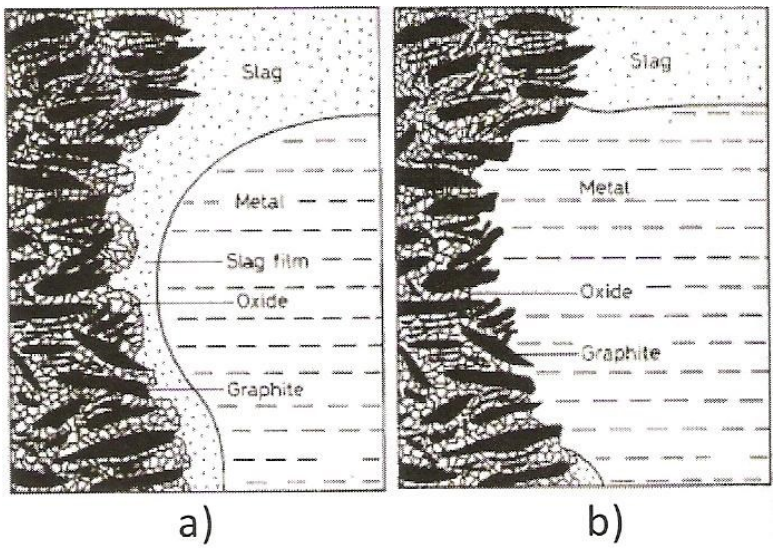

Figure 2. Local corrosion of the refractory at the slag – liquid steel interface. [4]

2.6. Preheating of the refractory. Protection of the refractory from decarburization.

Decarburization is the main wearing mechanism of the refractory during preheating of the ladle. Decarburization leads to increased porosity of the refractory. Antioxidants are used to decrease the decarburization rate of the refractory. Kasimagwa (2014) [2] found out that a heat-resistant sealant (Calofer) was the best protection against decarburization during preheating of the ladle. Refractory wear during preheating affects the steel quality because corrosion resistance is decreased due to decarburization. Dissolution of the refractory to the slag phase is enhanced at higher temperatures. Kasimagwa (2014) [2] says that the dissolution rate of the MgO-C refractory into the liquid slag increases when MgO content in the slag is low. The difference of the MgO content between the slag at the interface and the bulk is the driving force of the dissolution of the refractory into the liquid slag. [2]

2.7. Mixing

The purpose of the mixing is to achieve homogeneous temperature and composition of the liquid steel throughout the whole bath. Mixing in the ladle is done usually by stirring the liquid steel (and the slag) via argon gas bubbling. Stirring with argon gas can be done with submerged top lance or by porous plug in the bottom of the ladle. Argon gas is used because argon is inert gas. In gas stirred ladles the homogenization via mixing is caused by dissipation of buoyant energy of the injected gas. Mixing gets faster when porous plug is placed off-center on the bottom of the ladle. The placement of the plug/plugs as well as the shape and material of the plug affects the mixing time. The shape and the material affects in a way that, e.g., capillary plugs can be infiltrated easier than other plug shapes by liquid steel which affects the argon gas pressure. [1] Mass transfer between metal and slag is impeded when the porous plug is located off-center. Slag – liquid steel emulsification is increased when plug in the bottom of the ladle is located in the center of the bottom. [6]

Stirring in the ladle homogenizes composition and temperature of the molten steel and slag. The melt can also be mixed using electromagnetic stirring (EMS). Stirring also

enhances removal of inclusions from the molten steel. Steel-slag interactions are also facilitated. [1]

2.8. Desulfurization

Desulfurization is a process where sulfur is removed from the liquid steel. Desulfurization is based on sulfide formation and removal from the steel. Sulfur is bound in the basic top slag as CaS. Sulfur is harmful element for many steel grades and usually liquid steel is desulfurized in the secondary metallurgy phase. The progress of desulfurization process depends on the temperature of the slag and the steel as well as composition of the slag. Slag must be refining slag so that sulfur can be removed into the slag. Aluminium killed steels are easier to desulfurize than silicon killed steels because oxygen potential is higher in silicon killed steels. Desulfurization happens with contact between liquid steel and slag. Stirring by argon gas bubbling is the better choice for desulfurization. The more contact area liquid steel and slag have the faster is the desulfurization process. [5]

Desulfurization reaction is often written as in equation

$$[S] + (CaO) = [O] + (CaS). \quad (2)$$

Ability of slag to receive sulfur is described as "sulfur capacity". $C_S^{'}$ is the ability of the slag to receive sulfur from the molten steel and is calculated with equation

$$C_S^{'} = w_{S_s} \frac{a_{[O]}}{a_{[S]}}, \quad (3)$$

where w_{S_s} is the sulfur content in the slag in weight percent (w-%), $a_{[O]}$ is the oxygen activity in the liquid steel and $a_{[S]}$ is the sulfur activity in the liquid steel. [5]

2.9. Dephosphorization

Dephosporization is a process where phosphor is removed from the liquid steel. Phosphor is also a harmful element for many steel grades and dephosphorization is widely used process. Phosphor is trapped in the slag and the purpose of the slag is to

prevent the reversion of phosphor as in entrapment or dissolution of phosphor into the liquid steel. [1]

2.10. Reheating of the bath

Temperature control of the liquid steel is important for quality of the steel as well as for minimizing operating costs. Steel can be reheated via arc reheating or chemical reheating by adding aluminium and oxygen into the bath. With arc reheating the heating is accomplished by electrode lances immersed into the slag. [7]

Reheating can also be accomplished by chemical reactions between aluminium and oxygen which generates heat. Both reheating procedures are local and therefore need stirring of the liquid steel to homogenize the temperature in the bath. With chemical reheating also alumina inclusions must be removed to the top slag so that the quality of the steel does not suffer from the inclusions. [7]

Temperature of the liquid steel right before casting is crucial to solidification structure. Superheat of over 25 – 30 °C promotes columnar structure. Columnar structure has detrimental effects on quality of the steel. Columnar structure promotes possibility of internal cracks and bigger centerline macrosegregation and porosity. [7]

2.11. Deoxidation

Deoxidation process can be divided into three consecutive steps: formation of the critical nuclei, growth of the inclusions and flotation out of the melt. Homogeneous formation of the nuclei can be achieved if there is high supersaturation of the reactants. The assumption that deoxidation reactions are fast compared to other rate controlling phenomena is generally accepted. Growth of the inclusions is explained by collisions between the inclusions. Flotation of inclusions out of the melt is due to buoyancy of the inclusions. [1]

Liquid steel can be deoxidized with ferromanganese, ferrosilicon, silicomanganese and aluminium. Steels can be named after the deoxidizing procedure to non-killed, semi-killed or killed steel. Killed steels are deoxidized by aluminium to achieve minimum

amount of dissolved oxygen in the liquid steel. Deoxidation rate and final oxygen content in the liquid steel depends on the properties of the deoxidizer and the deoxidation products. The amount of removal of non-metallic inclusions is highly dependent on stirring of the liquid steel. [1]

2.12. Alloy additions

The adding of the metals or alloys can be done in many different stages of the steelmaking process, e.g. during tapping, in the ladle furnace or during vacuum degassing. The stage depends on the properties of the material to be added and the process route. The addition material can be injected into the melt in many different forms such as filled bag, wire or powder. The size of the addition depends how fast the addition should melt or dissolve into the liquid steel or into the slag. [1]

2.13. Calcium treatment

Calcium treatment is mainly done for modification of aluminium inclusions in aluminium killed steels. Calcium treatment modifies the alumina inclusions so that it prevents nozzle clogging and in the rolling of the steel calcium treated inclusions behave better. Alumina and silica inclusions change their composition and shape with calcium treatment and they are converted into a liquid calcium aluminates or calcium silicates. The control of the shape and composition of the inclusions is also called as a control of inclusion morphology. Calcium is usually added into the steel melt as a cored wire. Cored wire was developed for adding the calcium to the liquid steel because calcium is much lighter than the liquid steel and the boiling point of calcium is lower than the temperature of the steel. Therefore means for adding calcium as deep into the liquid steel was needed. The ferrostatic pressure in the bottom of the ladle is high enough to prevent calcium to evaporate. Sulfides can be also treated with calcium, e.g. manganese sulfide particles. Manganese sulfides precipitate in the grain boundaries but it can be prevented with inclusion morphology control with calcium treatment of the manganese sulfides. [1]

Additions to the molten steel can be added by wire feeding. Wire feeding is used if addition is less dense than the molten steel. Light addition in itself would float to the surface and would not react with the steel as desired. [1]

When ferrostatic pressure is higher than the vapor pressure of the gas the substance will form liquid globules. These liquid globules rise much slower than the gas and the contact time with the liquid metal is increased. [8]

Optimum release point of the powder is as deep as possible because of the low density of the powder and the fact that magnesium and calcium release gases. Low density substances and gases will rise to the surface due to buoyancy. Contact time of the powder substance with the liquid metal is desired to be as long as possible. The deeper the powder is injected the longer the contact time. [1]

2.14. Vacuum degassing

Easily evaporating impurities are removed from the liquid steel with vacuum degassing. Nowadays ultra-low carbon (ULC) steels and interstitial free (IT) steels can be made with vacuum degassing. Very low hydrogen, nitrogen and carbon contents in the liquid steel can be achieved via degassing of the liquid steel. There are two types of degassing procedures which are recirculating and non-recirculating systems. Aluminium usage can be minimized by deoxidizing the steel with vacuum carbon deoxidation. Carbon reacts with the oxygen to make carbon monoxide, as in equation

$$[C] + [O] \rightleftharpoons CO(g), \qquad (4)$$

which is then removed.

Nitrogen degassing can be done if the steel is fully killed and the sulfur content is low enough. Hydrogen can cause or assist cracking in steel. Hydrogen is removed from the steel with vacuum degassing. The relationship with partial pressure of hydrogen (p_{H_2}) and the concentration of hydrogen in liquid steel ($[ppm\ H]$) is presented in equation

$$\log\left(\frac{[ppm\ H]}{\left(p_{H_2}\right)^{½}}\right) = -\frac{1900}{T} + 2.423 \qquad (5)$$

where T is the temperature. [9]

Table 1. At temperature T = 1600 °C relationship between dissolved hydrogen concentration in steel and hydrogen pressure is given. [9]

pH_2 / atm	ppm H
1.0	25.6
0.1	8.1
0.01	2.56
0.001	0.81

Modern vacuum degassers can attain pressures p_{H_2} = 0.001. Pressures this low can be attained only near surface of the steel. At the bottom of the ladle there is ferrostatic pressure around 2 atm, which in relation to dissolved hydrogen concentration gives around 57 ppm hydrogen in steel. To fully degas the molten steel high circulation rate is required. Mass transfer during degassing controls the rate of the hydrogen removal. The degassing rate for all elements (H,N,C,O) can be increased by lowering the atmospheric pressure above the melt and by increasing the mixing in the melt. [1]

3. Inclusion models done by different authors

In this section/chapter different models are described and lightly interpreted. The point is to find ideas and methods for the online model. Before making an online model it is needed to look through models made by others.

3.1. Model by Harada et al.

Harada et al. [10][11] have made a kinetic model to predict the compositions of metal, slag and inclusions during ladle refining. In the introduction of their article [10] Harada et al. presented that in the past many authors assumed that the reactions in the ladle treatment were in an equilibrium state. Because the chemical composition of inclusions is non-uniform and the oxide phase is different for slag and inclusions the entire ladle treatment system does not reach the equilibrium. Therefore equilibrium theory is not by itself enough to model the ladle treatment process and reaction kinetics must be included in the model. The purpose of the model by Harada et al. [10] was to “clarify the mechanism of the composition change in steel, slag, and inclusion in

the ladle refining process" by "a kinetic model that considers the reaction between the metal and the slag as well as that between refractory/slag and metal/inclusion."

3.1.1. General overview of the model

Harada et al. [10][11] made a kinetic model to predict the compositions of liquid steel, slag and the inclusions during ladle refining. They considered following reactions:

- Reactions between liquid steel and the slag
- Reactions between the liquid steel and the inclusions originating from the slag
- The deoxidation reaction caused by the addition of alloying materials
- Dissolution of the refractory into the slag phase
- Formation, flotation and agglomeration of the inclusions

Harada et al. also separated slag and the liquid steel phases into interface and bulk zones.

In Figure 3 flow chart of the model by Harada et al. is presented.

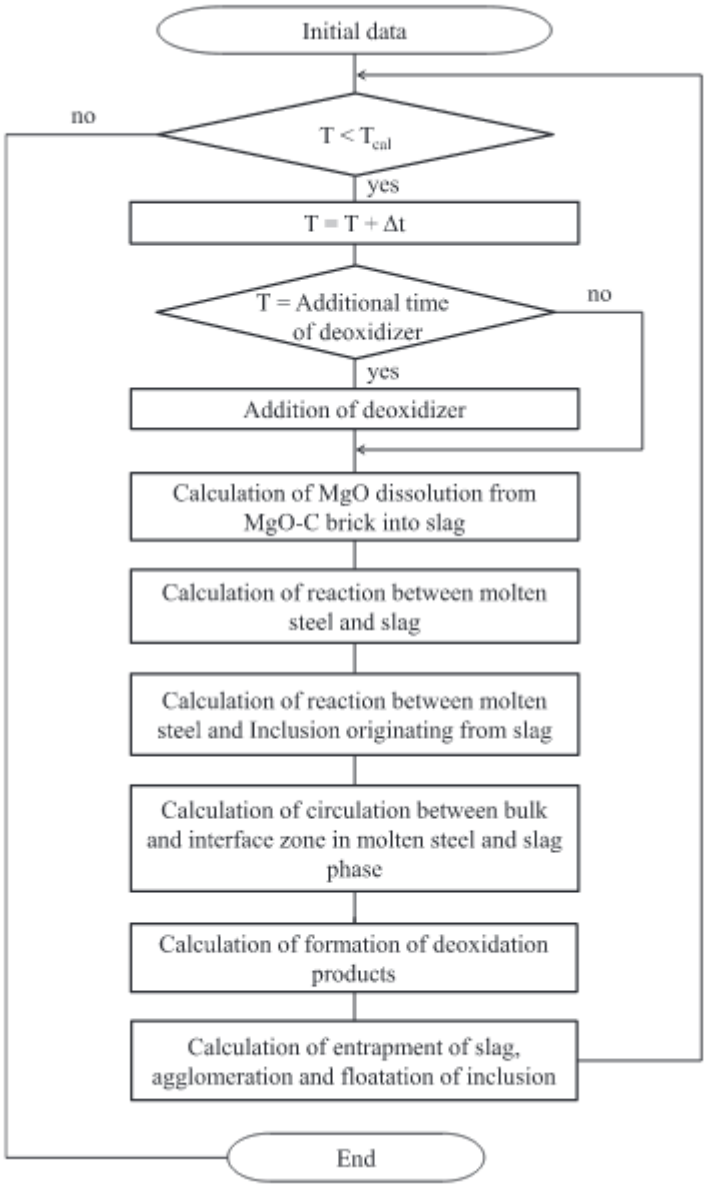

Figure 3. Flow chart of the model made by Harada et al. [10]

The calculation steps are presented in Figure 3, where it can be seen that addition of deoxidizer is considered first. Then refractory dissolution into the slag is computed. Reactions between liquid steel and slag are followed with reactions between liquid steel and inclusions originating from slag. Circulation of liquid steel and slag phases is computed. Then formation of deoxidation products is computed and lastly entrapment of slag as well as flotation and agglomeration of inclusions. This calculation scheme is looped until time used in calculations (T) goes over calculation time (T_{cal}) ($T > T_{cal}$). Harada et al. used time interval of 0.1 s but with reactions between liquid steel and

inclusions originating from slag time interval used was 0.005 s in order to improve the calculation stability.

3.1.2. Circulation

Harada et al. [10] made their circulation model by using perfect mixing time. They separated slag and the liquid steel phases into interface and bulk zones. In each phase zones are circulated at constant rate and phases are stirred by argon gas stirring. This is illustrated in Figure 4.

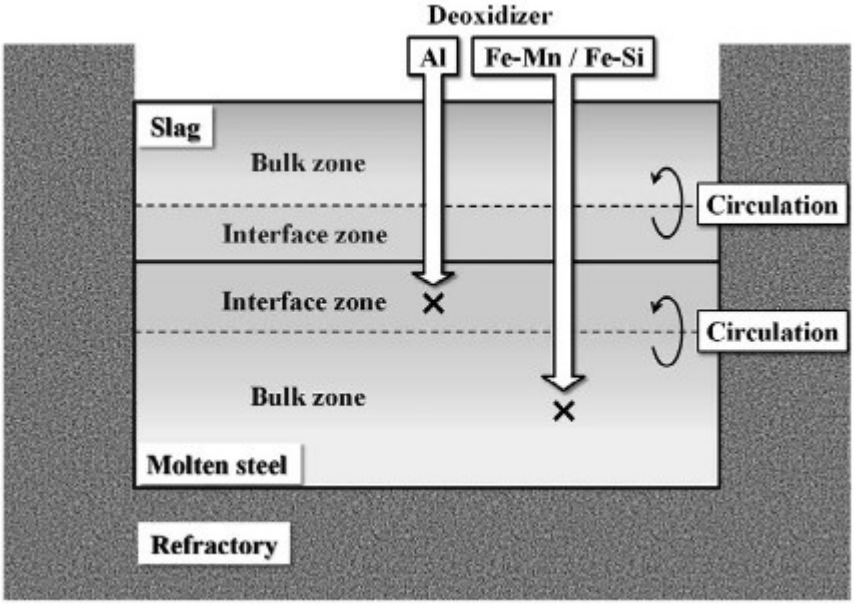

Figure 4. Circulation in the liquid steel and the slag in the model by Harada et al. [10]

Perfect mixing time is calculated with equation

$$t_m = 100\left(\frac{\left(\frac{d_v^2}{h_v}\right)^2}{\dot{\varepsilon}}\right)^{0.337}, \qquad (6)$$

where t_m is the perfect mixing time (s), d_v is the diameter of the bath (m), h_v is the bath depth (m) and $\dot{\varepsilon}$ is the stirring energy (W/t). [10]

Circulation rate of liquid steel is calculated with equation

$$v_m = \frac{W_m}{3t_m}, \tag{7}$$

where v is the circulation rate (t/s), W is the weight (t) and $(\,)_m$ indicates the value in liquid steel phase. It is assumed that each zone becomes uniform after three full circulations. [10]

Circulation rate of slag is a function of mass ratio between slag and liquid steel and is calculated with equation

$$v_s = v_m \left(\frac{W_s}{W_m}\right), \tag{8}$$

where $(\,)_s$ indicates the value in slag phase. [10]

Stirring energy is calculated with equation

$$\dot{\varepsilon} = \frac{6.18QT_m}{W_m}\left(\ln\left(1 + \frac{h_0}{1.46 * 10^{-5}P_a}\right) + \eta\left(1 - \frac{T_n}{T_m}\right)\right), \tag{9}$$

where Q is the argon gas flow rate (Nm^3/min),$(\,)_n$ indicates the value in gas phase, h_0 is the injection depth (m), P_a is the atmospheric pressure (Pa) and η is the fractional efficiency [12]. [10]

3.1.3. Interactions

Model by Harada et al. consists of several different interactions between different phases. Interactions are illustrated in Figure 5. Refractory dissolves only into the slag. Alloying materials dissolves into the liquid steel and forms deoxidation products. Liquid steel reacts with slag and inclusions originating from slag. Deoxidation products float into the slag and agglomerate with inclusions originating from slag. Inclusions originating from slag float into the slag.

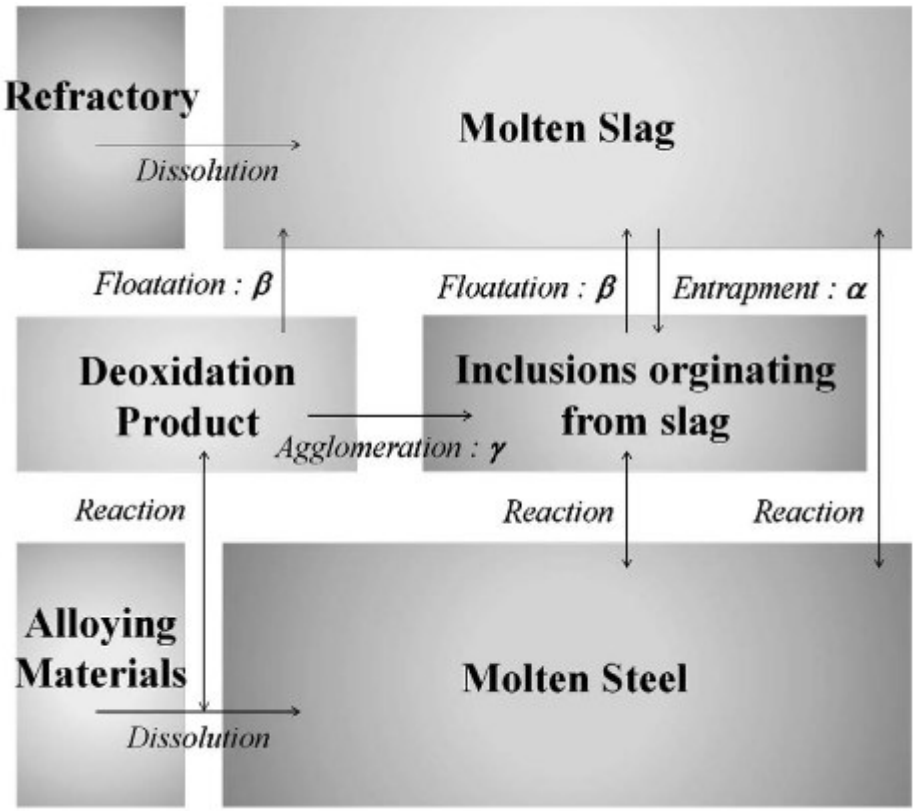

Figure 5. Illustration of interactions with different phases in the model by Harada et al. [10]

3.1.4. Refractory

Refractory dissolves into the slag but not into the liquid steel in model by Harada et al. Dissolution of refractory into the slag is considered because this phenomenon affects the composition of liquid steel indirectly with reactions between slag and the liquid steel. The reaction between the liquid steel and the refractory is not considered in this model because the dissolution rate of refractory into the liquid steel is lower than for the dissolution rate of refractory into the slag.

MgO was considered to be the refractory in this model. Mass transfer of MgO in the slag phase was assumed to be the rate-controlling step for dissolution of refractory into the slag. The driving force of the dissolution of refractory was assumed to be concentration difference between the MgO content and saturated MgO content in the slag phase. Dissolution rate or the decrease in thickness of the refractory wall is calculated with equation

$$-\frac{dr_r}{dt} = \frac{k_{MgO}}{100}\frac{\rho_s}{\rho_r}\{w_{MgO_s}{}^* - w_{MgO_s}\}, \quad (10)$$

where r_r is the refractory thickness (m), t is the time (s), k_{MgO} is the mass transfer coefficient of MgO in the slag phase (m/s), ρ is the density (kg/m^3), $(\,)_r$ indicates the value of refractory, $(\,)_s$ indicates the value in the slag phase and $(\,)^*$ indicates the saturated concentration. [10]

Mass transfer coefficient of the MgO in the slag phase is calculated with equation

$$k_{MgO} = \frac{0.0791 u^{0.7} D_{MgO}^{0.644}}{l^{0.3} v^{0.344}}, \quad (11)$$

where u is the characteristic velocity (m/s), v is the dynamic viscosity (m^2/s), D is the diffusion coefficient (m^2*s) and l is the characteristic length (m).

Harada et al. assumed the characteristic velocity as rising velocity of the liquid steel in the plume area created by injected gas and they determined characteristic length to be one-half power of the contact area between the slag and the refractory.

3.1.5. Reactions between liquid steel and slag

Reactions between liquid steel and slag were modeled by Harada et al. with coupled reaction model. When there are simultaneously multiple reactions occurring and the process is not in equilibrium coupled reaction model is necessary. Reactions are described with double film theory. At the interface equilibrium conditions are assumed.

Equation

$$[M] + n[O] = (MO_n) \quad (12)$$

presents oxidation reaction for element M in the liquid steel phase.

Molar flux density of element M (J_M (mol/m^{2}s)) is expressed in equation

$$\begin{aligned} J_M &= \left(\frac{k_m \cdot \rho_m}{100 M_M}\right)\{w_{M_m}{}^b - w_{M_m}{}^I\} \\ &= \left(\frac{k_s \cdot \rho_s}{100 M_{MO_n}}\right)\{w_{MO_{n_S}}{}^I - w_{MO_{n_S}}{}^b\}, \end{aligned} \quad (13)$$

where k is the mass transfer coefficient in the film layer (m/s), M_M is the atomic weight of element M (),$M_{MO_n}$is the molecular weight of oxide MO_n (), $(\,)^b$ indicates the value in the bulk, $(\,)^I$ indicates the value in the interface, and $(\,)_m$ indicates the value in the liquid steel. [10]

Molar flux density is defined as a mass transfer of M from liquid steel through the interface to the slag. Middle part of the equation expresses the molar flux of element M in the liquid steel phase. Right part of the equation expresses the molar flux of element M in the slag phase. The driving force of mass transfer is the concentration difference between the bulk phase and the interface. Bulk phase for middle part of the equation is the liquid steel and for the right side the bulk phase is the liquid slag. Molar flux density of element M into the interface is assumed to be equal as the molar flux density of element M out of the interface.

Equilibrium partition ratio for each element M (E_M) can be calculated with equation

$$E_M = \frac{{w_{MO_n}}_S^{\ I}}{{w_{M_m}}^I \cdot a_O^{In}} = \frac{100CM_{MOn}f_M K_M}{\rho_s \gamma_{MOn}}, \qquad (14)$$

where a_O is the oxygen activity, C is the total number of moles in the liquid slag phase, f_M is the activity coefficient of element M, K_M is the equilibrium constant of equation 12 and γ_{MOn} is the activity coefficient of MO_n. E_M describes how the element M is distributed between liquid steel and liquid slag in the interface. [10]

Molar flux densities for Fe and O are calculated with equations

$$J_{Fe} = \left(\frac{k_s \rho_s}{100M_{FeO}}\right)\left\{{w_{FeO}}_S^{\ I} - {w_{FeO}}_S^{\ b}\right\} \qquad (15)$$

and

$$J_O = \left(\frac{k_m \cdot \rho_m}{100M_O}\right)\left\{{w_{O_m}}^b - {w_{O_m}}^I\right\}. \text{ [10]} \qquad (16)$$

Equation

$$\sum J_M = 0 \qquad (17)$$

indicates that the total molar flux densities of cations and anions must be equal. The equation expresses electrical neutrality.

Desulfurization reaction is presented in equation 18.

$$(CaO) + [S] = (CaS) + [O] \tag{18}$$

Molar flux density for sulfur is calculated with equation 19 [10].

$$J_S = \left(\frac{k_m \cdot \rho_m}{100 M_S}\right)\left\{{w_{S_m}}^b - {w_{S_m}}^I\right\} = \left(\frac{k_s \cdot \rho_s}{100 M_{CaS}}\right)\left\{{w_{CaS_s}}^I - {w_{CaS_s}}^b\right\} \tag{19}$$

Equilibrium partition ratio for sulfur is calculated with equation

$$E_S = \frac{\left\{{w_{CaS_s}}^I \cdot a_O^I\right\}}{\left\{{w_{S_m}}^I {w_{CaO_s}}^I\right\}} = \frac{\left\{{w_{S_s}}^I \cdot \frac{a_O^I}{a_S^I}\right\}\left(\frac{M_{CaS}}{M_S}\right) f_S}{{w_{CaO_s}}^I} = \frac{C_S'\left(\frac{M_{CaS}}{M_S}\right) f_S}{{w_{CaO_s}}^I}. \text{ [10]} \tag{20}$$

Activities of components in the slag phase were calculated in every step of calculation with FactSage6.3 which was linked to developed program through ChemApp.

The mass transfer coefficient for liquid steel phase is calculated with equation

$$log k_m = 1.98 + 0.5 \log\left(1000 \dot{\varepsilon} \frac{h_v^2}{d_v}\right) - \frac{125000}{2.3RT}, \tag{21}$$

where R is the gas constant (J/molK). For each element the mass transfer coefficient is assumed to be the same. [10]

The mass transfer coefficient for slag phase is calculated with equation

$$k_s = \frac{k_m}{10}. \text{ [10]} \tag{22}$$

For slag phase it is assumed that the average mass transfer coefficient for slag phase is one tenth of the mass transfer coefficient for liquid steel, because diffusion coefficients for slag phase are 10-100 times smaller than for liquid steel phase. This average value is assumed to be the mass transfer coefficient for CaO in the slag phase.

Mass transfer coefficients for oxides in the slag phase are calculated with equation

$$k_{MO_n} = k_s \sqrt{\frac{D_{MO_n}}{D_{CaO}}}. \text{ [10]} \qquad (23)$$

It is assumed that the ratio between mass transfer coefficient of oxide and CaO is proportional to the one-half power of the ratio between diffusion coefficients.

3.1.6. Reaction between liquid steel and the inclusion originating from slag

Inclusions originating from the slag are the inclusions resulting from the entrapment of top slag in the liquid steel. Reaction area with reactions between liquid steel and the inclusions originating from slag is calculated to be the surface area of one inclusion particle assumed to be spherical (10µm in diameter) multiplied with the number of inclusions. Harada et al. does not present how they calculate or assume the number of inclusions.

Mass transfer coefficient of the inclusion originating from slag is calculated with equation

$$k_m = 2\left(\frac{D_m u_{slip}}{\pi d_p}\right)^{\frac{1}{2}}, \qquad (24)$$

where u_{slip} is the slip velocity between the inclusion particle and the liquid steel (m/s), d_p is the diameter of the inclusion particle (m) and $(\,)_p$ indicates the value of the inclusion particle. Slip velocity between the inclusion particle and the liquid steel is calculated with equation

$$u_{slip} = \left(\frac{4g^2(\rho_m - \rho_p)^2 d_p^3}{225\mu_m \rho_m}\right)^{\frac{1}{3}}, \qquad (25)$$

where g is the gravitational acceleration (m/s^2). [10]

Equations above are used to calculate the k_m. Mass transfer coefficient for liquid oxide phase is calculated with equations 22 and 23. If the original result from equation 24 is used the composition change of inclusions originating from slag is too high and the calculation is unstable. Therefore in actual calculation Harada et al. divided the result from equation 24 by 50 to make the calculation stable.

Inclusion size is very important parameter in this study because it affects so many other parameters: slip velocity and the mass transfer coefficient of the inclusion originating from slag as well as the reaction area between liquid steel and inclusion originating from slag. Size distribution for inclusions originating from slag is not known. Harada et al. assumed that the size of the inclusion originating from slag is 10 µm. Future study for Harada et al. is to study the size distribution of the inclusions originating from slag.

3.1.7. Formation, coagulation and flotation of the inclusions in the slag phase.

Two sources of inclusions are considered in the model by Harada et al. They are entrapment of slag in the liquid steel and deoxidation products. MnO-SiO_2, Alumina (Al_2O_3), MgO·Al_2O_3 spinel and CaO-Al_2O_3 are considered to be the deoxidation products.

Deoxidation reactions are presented in equations 26 to 29. Equation 26 is the oxidation reaction for pure alumina.

$$2[Al] + 3[O] = Al_2O_3(s) \qquad (26)$$

For simplicity in order to calculate the deoxidation equilibrium Harada et al. assumed that mole fractions and activities of CaO, MgO and SiO_2 are constant. These constants are presented in Table 2.

$$[Ca] + [O] = CaO(in\ CaO - Al_2O_3) \qquad (27)$$

$$[Mg] + [O] = MgO(in\ MgO - Al_2O_3) \qquad (28)$$

$$[Si] + 2[O] = SiO_2(in\ MnO - SiO_2) \qquad (29)$$

Table 2. Mole fractions and activities of CaO, MgO and SiO_2. [10].

	Mole fraction	Activity
CaO	0.525	0.2
MgO	0.5	0.08
SiO_2	0.575	0.4

The free energy change of reaction is calculated with equation 30.

$$\Delta G = \Delta G^0 + RTlnK \quad (30)$$

Equilibrium constants for reactions 26 to 29 are presented in equations

$$K_{Al_2O_3} = \frac{a_{Al_2O_3}}{a_{Al}^2 a_O^3}, \quad (31)$$

$$K_{CaO} = \frac{a_{CaO}}{a_{Ca} a_O}, \quad (32)$$

$$K_{MgO} = \frac{a_{MgO}}{a_{Mg} a_O} \quad (33)$$

and

$$K_{SiO_2} = \frac{a_{SiO_2}}{a_{Si} a_O^2} \quad (34)$$

respectively.

Harada et al. does not present how they calculate the activities of the solute elements in the liquid steel.

After addition of the deoxidizer deoxidation reaction must be achieved. Harada et al. calculate the ΔG value for each reaction (equations 26 to 29). The reaction that has the smallest negative ΔG value is deemed to occur and the concentrations of the reacted elements, e.g. Si and O, are changed slightly. This procedure is repeated until the ΔG value for all reactions is positive because reactions do not go further anymore. Harada et al. does not present how much is slightly as in how much they change the concentrations in each step.

Harada et al. assumed that the volume ratio between slag and the entrapment of slag into the liquid steel is constant. This can be interpreted so that every second some slag is entrapped into the liquid steel. Part of the deoxidation products (inclusions from deoxidation reactions) agglomerates with inclusions originating from slag. Also part of

the deoxidation products as well as inclusions originating from slag are floated into the top slag. Volume ratio of deoxidation products which agglomerates with inclusions originating from slag, volume ratio of deoxidation products that float in the slag as well as volume ratio of inclusions originating from slag that floats in the slag are assumed as constants.

To analyze the value of the constants Harada et al. did sensitivity analysis [11] for ratio of the entrapment of slag into the liquid steel to the total amount of slag (H_α), ratio of the flotation of the deoxidation products or inclusions originating from slag to the total amount of deoxidation products or inclusions originating from slag (H_β), ratio of the agglomeration of deoxidation products with the inclusions originating from slag to the total amount of deoxidation products (H_γ) and ratio between the volume of bulk zone to the total amount of liquid steel and slag (V_b/V). In Table 3 analyzed values for H_α, H_β, H_γ and V_b/V are presented as well as the chosen value for the constants.

Table 3. Sensitivity analysis made by Harada et al. [11] for acquiring optimal value for constant ratios in their model.

	Analyzed ratios	Chosen value
H_α	10^{-3}, 10^{-4}, 10^{-5}, 10^{-6}	10^{-6}
H_β	1, 0.1, 0.01	0.1
H_γ	1, 0.1, 0.01	1
V_b/V	0.9, 0.8, 0.7	0.8

Analyzed ratios for the constants were compared to the operational data and the chosen values represent the operational data the best.

3.2. Model by Shu and Scheller

Shu and Scheller [13][14] developed a model for online prediction of the amount and composition of inclusions in ladle treatment. Kinetic modeling of interface between slag and steel is challenging to model due to various reactions. Equilibrium modeling has been done for a long time and equilibrium modeling programs exist. Bulk steel and bulk slag are not in equilibrium and they are constantly reacting with each other. Shu & Scheller modeled slag-metal interface with following scheme. Thin layer on both side

of the slag-metal interface can be estimated to be in equilibrium or at least reactions close to interface can be modeled as such. Part of the bulk steel and bulk slag are calculated to be in equilibrium. Reaction products (equilibrium calculation results) are categorized to be part of the steel or slag and are added to the bulk steel or bulk slag respectively.

3.2.1. General overview of the model

Shu and Scheller considered following phenomena

- Mixing in the ladle
- Slag-liquid steel reaction
- Inclusion separation
- Refractory interactions with liquid steel and slag

In Figure 6 considered phenomena are illustrated.

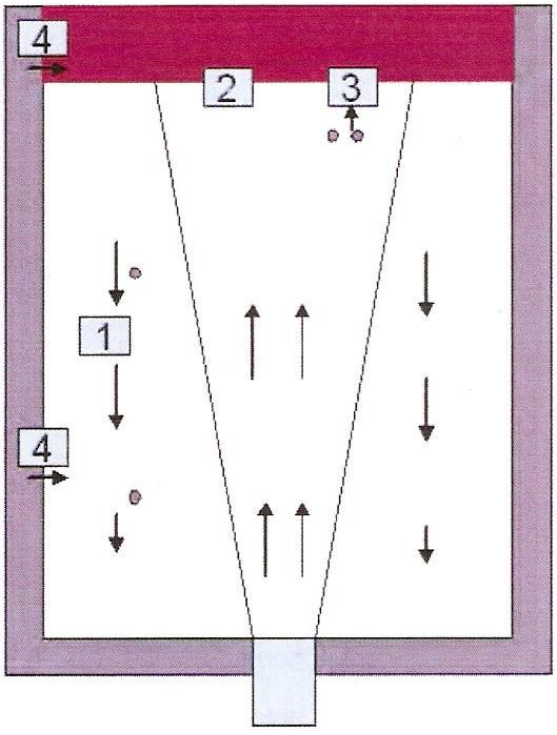

Figure 6. Illustration of the phenomena in the model. 1. Mixing, 2. Slag – Steel reactions, 3. Inclusion separation, 4. Reactions between refractory and slag / steel. [13]

They used SimuSage for basic unit operations (chemical reactor, mixer, splitter, iterator) and FactSage to acquire thermodynamic data of the phases (liquid steel, slag, inclusions and refractory lining). They assumed that temperature is uniform throughout the whole bath. The comparisons between calculated and industrial data show that the predictions of the present model are consistent with industrial practice [14].

3.2.2. Mixing

Shu and Scheller used tanks in series model for mixing which is illustrated at Figure 7. Plume due to gas stirring generates flow in the ladle. Liquid steel and non-metallic inclusions from plume are transferred into the Tank 1 due to the flow where it goes through Tank 2 and Tank 3 back to the plume. Plume also generates the flow in the slag. Slag1 and Slag2 transfer material between these two tanks.

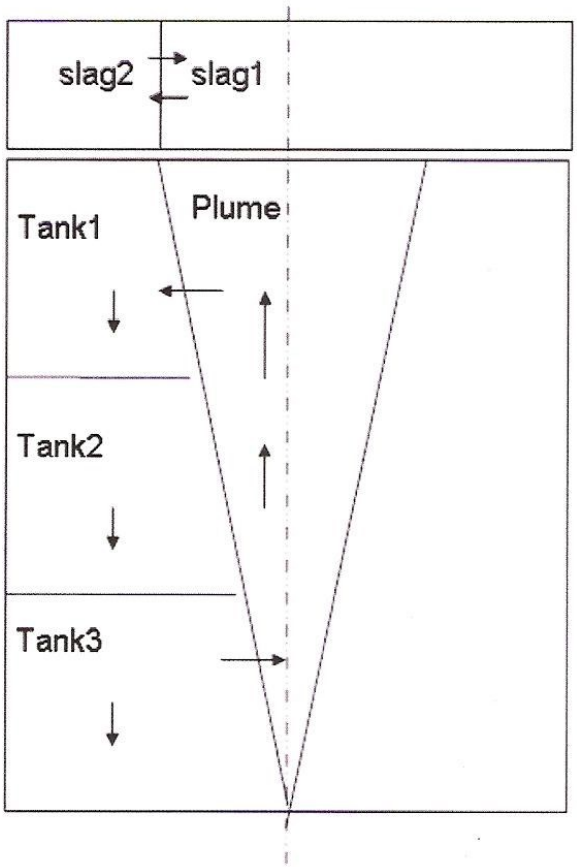

Figure 7. Schema of the tanks. [13]

The flow and the interactions between the different phases are illustrated in Figure 8. In addition to the flow and mixing Tanks 1 to 3 and Slag2 interact with the refractory lining. Tank 1 also interacts with Slag2. Plume interacts with Slag1 where the non-metallic inclusions are separated into the slag. Concentrations of inclusions are calculated in the mixing phenomenon with equation

$$C(N,t) = \frac{C(N,t-\Delta t)(M(N) - r_{mass}\Delta t) + C(N-1,t-\Delta t)r_{mass}\Delta t}{W(N)}, \qquad (35)$$

where C(N,t) is the concentration in tank N at time t, W(N) is the mass of tank N and r_{mass} is the mass recirculation rate (obtained from industrial trials). [13]

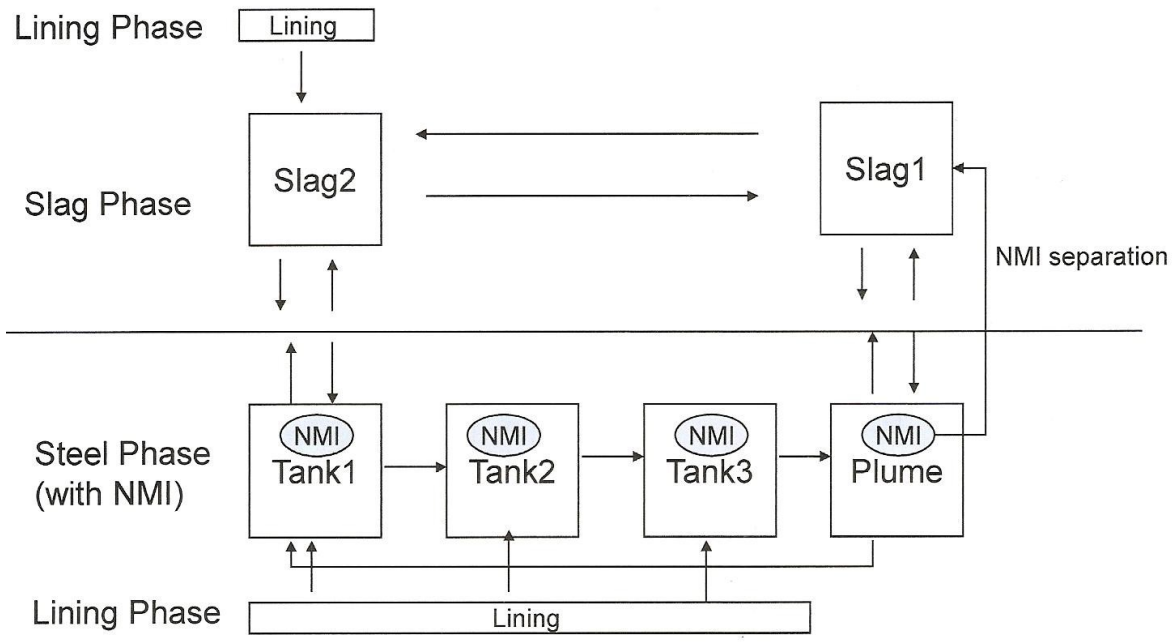

Figure 8. Schema of the model. All reactions are showed in this figure. Mixing, reactions in the interface, inclusion separation, refractory interaction. Non-metallic inclusions are notated as NMI. [13]

3.2.3. Slag-liquid steel reaction

Shu and Scheller modeled the slag – liquid steel reaction with following technique. Part of the bulk liquid steel and slag are reacting at the interface of the phases. The products of the reaction are divided into products for liquid steel and slag and they are added to the bulk liquid steel and slag.

The mass transfer coefficient of steel k_m and the mass transfer coefficient of slag k_s are employed to describe the kinetics of slag-steel reaction. [14]

Mass of the reacted steel is calculated with equation

$$W_m = k_m \rho_m A_I \Delta t, \qquad (36)$$

where A_I is the area of the interface. [13]

Mass of the reacted slag is calculated with equation

$$W_s = k_s \rho_s A_I \Delta t. \ [13] \qquad (37)$$

The combined mass of liquid steel and slag is constant before and after the reaction at the interface;

$$W_s + W_m = W_{s1} + W_{m1}.\ ^{[13]} \qquad (38)$$

Mass transfer coefficients are assumed to be constant through the whole ladle treatment. Mass transfer coefficients can be seen in Table 4.

Table 4. Data Shu & Scheller used in their calculations. Mass transfer coefficients and dissolution rates of refractory.[13]

	Value	**Unit**
k_m	0.002	m/s
k_s	0.001	m/s
$(dW_r/dt)_m$	0.0005	kg/(m^2/s)
$(dW_r/dt)_s$	0.001	kg/(m^2/s)

Reactions in the interface are calculated as illustrated in Figure 9. Splitter splits part of the bulk material as defined in equations 36 and 37. Splitted materials from liquid steel and slag react with each other. Reacted liquid steel and slag are calculated to be in equilibrium. The respective reaction products are added to the bulk steel and slag.

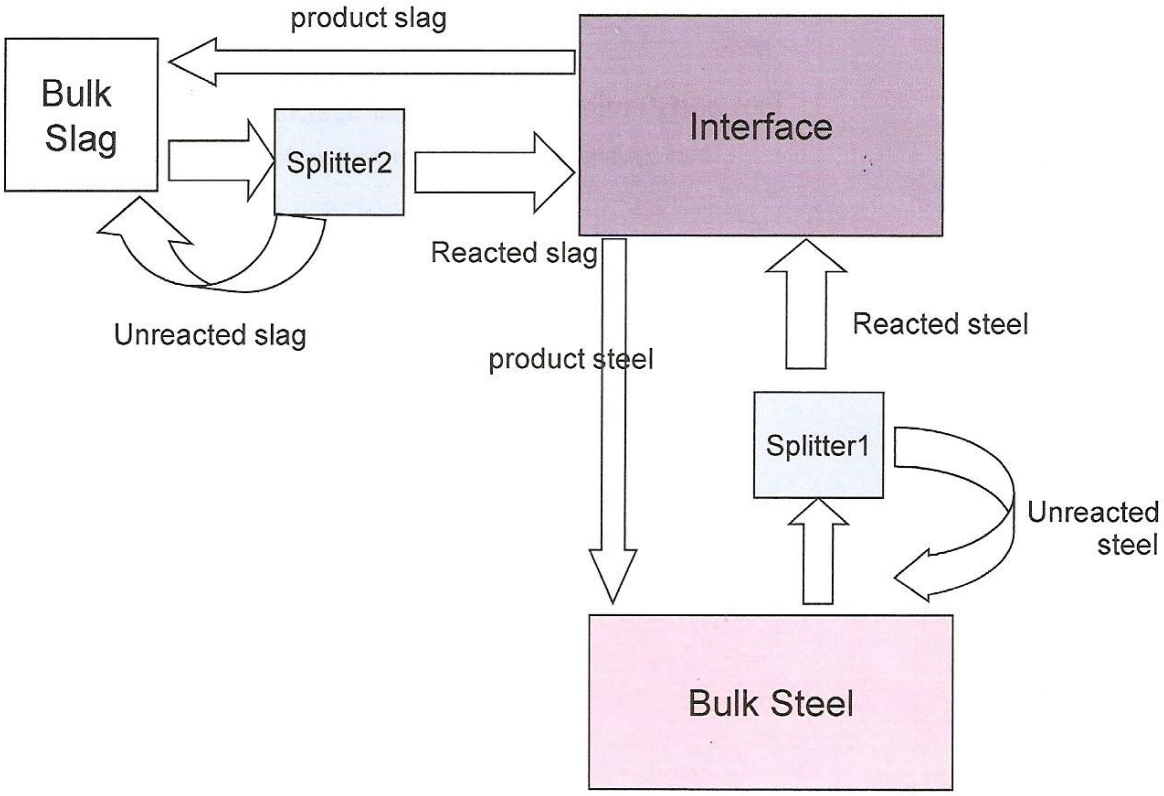

Figure 9. Schema of the Slag – Steel reactions. Splitters 1 and 2 divides bulk quantities to unreacted and reacted slag / steel. Reacted slag reacts with reacted steel in the interface. [13]

3.2.4. Equilibria

Shu & Scheller assumed there is a thermodynamic equilibrium between

- liquid steel and inclusions in each tank (tanks in the mixing model)
- slag and liquid steel at the interface (slag – steel interface)
- liquid steel and dissolved refractory material (tanks in the mixing model)

So in each step these relations are calculated to be in equilibrium between affected phases.

3.2.5. Refractory

A typical material used for lining is MgO-C brick. Lining material can enter the steel due to mechanical or chemical refractory erosion. A certain rate of dissolution of lining material is assumed on the basis of industrial data. Dissolution rate for lining into steel or slag can be estimated according to the loss of lining during ladle treatment. [14]

Refractory lining dissolves into each tank that is connected to the refractory lining. Tanks 1 to 3 and Slag2 in Figure 7 are connected to the refractory lining in their model. Dissolution rates of the refractory lining into the liquid steel and slag are assumed to be constants through the whole ladle treatment. Shu and Scheller used empirical industrial data for dissolution rates. Dissolution rates of refractory can be seen in Table 4.

3.2.6. Separation of inclusions

Separation of inclusions was taken into account in Shu & Scheller's model. Separation rate depends on nature of inclusions and process development. Separation of inclusions can be complex but as a simplification Shu & Scheller assumed in their model that inclusions follow steel flow while moving towards the slag – steel interface. This assumption is justified because of the small size of the inclusions. Most of them have a size <40 μm, and therefore the buoyancy force is negligible. Solid alumina and calcium aluminates can agglomerate quickly by collision, but liquid aluminates and Mg-Al spinels do not agglomerate as well or at all [15][16][17]. Liquid inclusions lack attraction force between colliding particles [15]. Solid alumina particles can easily separate into the slag but liquid inclusions do not separate as well [17][18]. Alumina and solid aluminates agglomerate, float and separate into the slag easier than liquid aluminates and Mg-Al spinel. Based on above information Shu & Scheller chose separation percentages for solid Mg-Al spinel and liquid inclusions to be 3 – 5 %. Separation percentage for alumina and alumina rich aluminate was chosen to be 20 % in the first 10 minutes after Al-addition and then fading out in the remaining period of treatment. [14]

3.3. Model by Bellot et al.

Bellot et al.[20] made a model to predict the amount of inclusions and their size distribution in the ladle (inclusion population). They used computational fluid dynamics (CFD) and population balance equations (PBE) to simulate the evolution of

inclusion population. The basis of the model made by Bellot et al. is the model made by Felice et al. [21].

In this work CFD part of the model by Bellot et al. is not presented in detail because it is computationally so slow that it would not be suitable for online model. On the other hand the PBE part of the model by Bellot et al. is presented in more detailed.

Bellot et al. calculated PBE with two different methods. They calculated 3-D and 0-D PBE. 0-D model reduced the computational effort a lot.

3.3.1. General overview of the model

The interactions that Bellot et al. [20] considered in their models for evolution of inclusion population are as follows:

- the collisions between inclusions (can lead to aggregation and agglomeration)
- the collisions with bubbles (can lead to flotation)
- the entrapment at the interface between the liquid bath and slag coverage
- the separation induced by gravity
- the entrapment at the ladle walls

Bellot et al. used the Fluent CFD code as a basis of their 3-D simulation model. They presented their development of the 3-D simulation model which takes into account the geometry of the industrial ladle and operating conditions.

They divided the presentation of their model into two parts.

1. Two-phase flow: turbulent gas-liquid flow. CFD
2. The behavior of oxide inclusions. PBE with 3-D and 0-D geometry

3.3.2. Hydrodynamic modeling of the liquid-gas mixture

Bellot et al. modeled the liquid – gas flow with basis of Fluent code. They used Eulerian-Eulerian scheme to simulate the two-phase liquid-gas flow. They chose Euler-Euler scheme because the main advantage (over Euler-Lagrange) of that scheme is that

inclusion transport coupled with population balance can be calculated without the use of post-processing operations [21].

Transport equations define the flow. Equation

$$\frac{\partial}{\partial t}(\alpha_k \rho_k) + \nabla \cdot (\alpha_k \rho_k u_k) = 0 \qquad (39)$$

is the continuity equation for phase k, where $()_k$ index stands for each phase, liquid l and gas g, α is the retention rate (volume fraction of the phase in the mixture) and **u** is the average velocity vector. [20] Equation

$$\frac{\partial}{\partial t}(\alpha_k \rho_k \boldsymbol{u_k}) + \nabla \cdot (\alpha_k \rho_k \boldsymbol{u_k} \boldsymbol{u_k}) = -\alpha_k \nabla p - \nabla \cdot (\alpha_k \tau_k) + \alpha_k \rho_k \boldsymbol{g} + \boldsymbol{F_k} \qquad (40)$$

is the momentum transfer equation for phase k, where τ is the tensor of viscous stresses, p is the local pressure and **F** is the interaction forces between the two phases. [20]

External forces are coupled for two sets of equations for liquid steel and the argon gas bubbles. Forces are opposite due to Newton's III law (F_l = -F_g). Interaction forces are divided into: drag force, lift force, force due to added mass effect and force due to turbulent dispersion.

Bellot et al. calculated the turbulence of the liquid steel phase with the standard k-ε model.

Source terms are added into the equations 39 and 40 at the inlet and outlet to simulate the gas injection and degassing.

Bellot et al. defined many user defined functions (UDF) to take into account the specific features of the hydrodynamic model.

Bellot et al. validated their CFD part of the model by comparing their model with values found from literature. The validation was successful because they found in the literature that the liquid steel velocities are consistent with the magnitude found for equivalent industrial configurations.

They also made experimental measurements to validate their simulation of mixing. In their experimental set up they used copper as a chemical tracer and measured the time necessary for a full homogenization of the liquid phase.

They found out that in comparison with the experimental set up their model underestimates the bath mixing time but the order of magnitude is in agreement.

They found strong dependence of mixing with the initial tracer location. They explained that this might be because of the solidified shell formation/effect is different in different initial tracer locations, and their model does not take into account of the solidified shell formation.

3.3.3. Modeling the inclusion behavior

The behavior of the inclusion population, defined by a distribution function of particle size, is described by the PBE. N_i is the number of inclusions of class "i" per m^3 of liquid steel. Class "i" contains all inclusions that have a volume between v_i and v_{i+1}.

PBE for 3-D case is presented in equation

$$\frac{\partial}{\partial t}(\alpha_l N_i) + \nabla \cdot (\alpha_l \boldsymbol{u}_l N_i) = \alpha_l(B_i - D_i) - \alpha_l Z_{bi} - S_i, \qquad (41)$$

where S_i is the inclusion gravity separation term, B_i is the birth rate, D_i is the death rate and Z_{bi} is the flotation term. Left side of the equation represents the macroscopic transport phenomena of inclusions, and right side represents the mesoscopic phenomena such as bubble-inclusion (flotation Z_{bi}) and inclusion-inclusion (aggregation B_i and D_i) interactions. [20]

The transient solution for equation 41 Bellot et al. calculated by dividing the equation into a transport and collision part of the equation. First the transport equation is solved and secondly the population balance equation is solved in each control volume. Transport equation is

$$\frac{\partial}{\partial t}(\alpha_l N_i) + \nabla \cdot (\alpha_l \boldsymbol{u}_l N_i) = 0 \qquad (42)$$

and it is solved with finite volume method (FVM).

Then population balance equation is

$$\frac{\partial}{\partial t}(\alpha_l N_i) = \alpha_l(\mathrm{B_i} - \mathrm{D_i}) - \alpha_l Z_{bi} - S_i \qquad (43)$$

and it is solved with cell average method.

Cell average technique is a technique in which new formed particles (due to a e.g. agglomeration of other particles) are divided into a different classes by volume of the new particles. PBE keeps in count how many particles are represented by a certain class "i" with N_i. N_i is the amount of inclusions in a class "i". Class "i" is the group of inclusions that have a volume of $[v_i, v_{i+1}[$. When new particles form to a class "i" volume average is calculated. If the volume average is between $[v_{i-1}, x_{i-1}[$, where x_{i-1} is the representative size of (i-1)th cell ($x_{i-1} = (v_i+v_{i-1})/2$), there is no birth at ith cell due to these new particles. On the other hand if the volume average is between $[x_{i-1}, v_i[$ there is a birth contribution to a ith cell due to these new particles. This is illustrated at Figure 10. Basically volume average is calculated in order to know how to distribute the new particles to different classes (cells). The distribution is done so that total mass and the number of particles are preserved. [22]

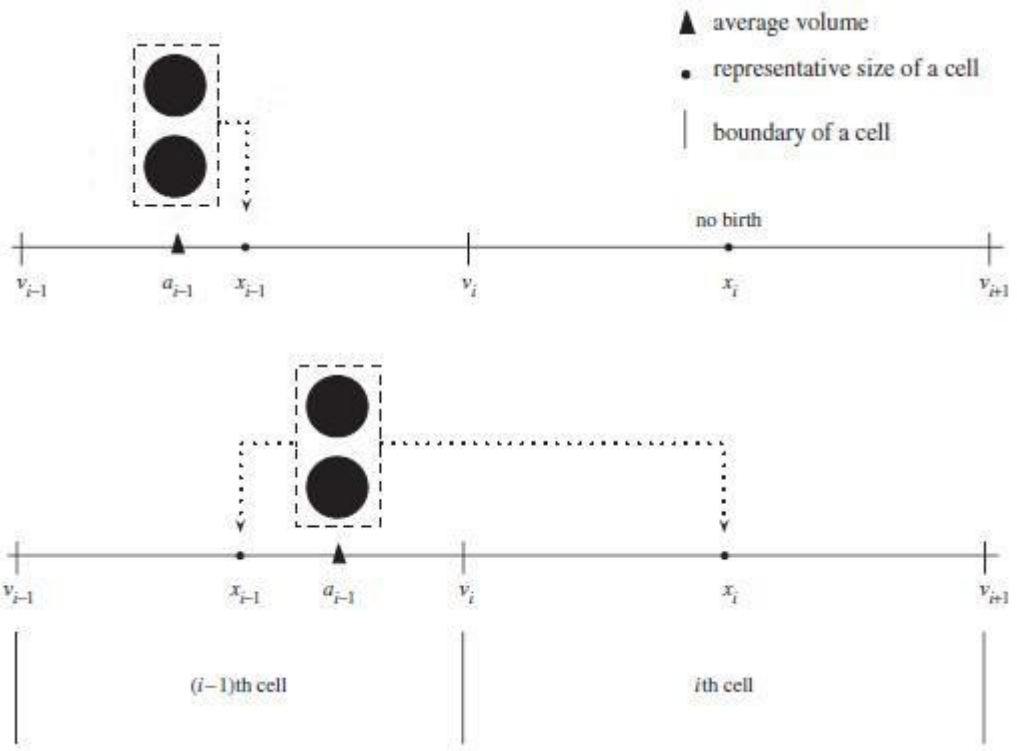

Figure 10. The Cell average technique. [22]

Birth rate is determined by the sizes of the smaller particles colliding and agglomerating into a particle size i. Death rate is the rate that the particle size class i particles collide and agglomerate with other particles to form a bigger particles.

Birth rate defines how many inclusions of class “i" is formed and death rate defines how many inclusions of class “i" are agglomerating into a bigger inclusion. Birth and death rates are shown in equation

$$B_i - D_i = \frac{1}{2}\sum_{j+k=i} \beta_{jk} N_j N_k - N_i \sum_{j=1} \beta_{ij} N_j, \qquad (44)$$

where β_{jk} is the collision frequency between size classes j and k. [23] Bellot et al. used collision frequency proposed by Zaichik et al. [24].

Flotation rate is presented in equation

$$Z_{bi} = E_c \alpha_l \beta_{bi} N_b N_i \qquad (45)$$

where E_c is the collision efficiency, N_b is the numeral density of bubbles and β_{bi} is the flotation frequency. [21]

Flotation frequency is calculated with equations 46[21] to 48[21].

$$\beta_{bi} = \beta_{det} + \beta_{turb,i} \tag{46}$$

where β_{det} is the deterministic frequency (bubble-inclusion slipping velocity) and $\beta_{turb,I}$ is the stochastic frequency (turbulent agitation of particles).

$$\beta_{det} = \frac{\pi d_b^2 U_{gl}}{4} \tag{47}$$

where d_b is the equivalent gas bubbles diameter and U_{gl} is the average sliding liquid-bubble velocity.

$$\beta_{turb,i} = \sqrt{\frac{8\pi}{15}} \left(\frac{d_b + d_{pi}}{2}\right)^3 \left(\frac{\varepsilon_l}{\nu_l}\right)^{0.5} \tag{48}$$

where d_{pi} is the particle diameter representative of the class i.

Bellot et al. assumed that the particles have a shape of spherical cap. Collision efficiency for this kind of particle is defined in equation

$$E_c = 1.7 \frac{d_{pi}}{d_b}. \text{ [21]} \tag{49}$$

Separation induced by gravity is calculated with equation

$$S_i = \nabla \cdot (\alpha_l \boldsymbol{u_s} N_i) \tag{50}$$

where $\mathbf{u}_s$ is the vertical Stokes velocity in the case of small inclusions whose Re < 1. [20] Vertical Stokes velocity is calculated with equation

$$\boldsymbol{u_s} = -\frac{d_{pi}^2 (\rho_l - \rho_g) g}{18 \mu_l}. \text{ [21]} \tag{51}$$

The inclusion entrapment at the liquid metal/slag interface is modeled following the approach based on a deposition law which is adapted to a free liquid surface condition by Xayasenh [25], equation 52[21] and 53[21].

$$\varphi_i = -\alpha_l \boldsymbol{u_{d,i}} N_i \tag{52}$$

where φ is the out-flow density and $\mathbf{u_d}$ is the adimensional inclusion deposition velocity.

$$\boldsymbol{u_{d,i}} = \left(0.057Sc^{-\frac{2}{3}} + 4.5 \cdot 10^{-4}\boldsymbol{\tau_p^{+2}}\right)\boldsymbol{u^*} \qquad (53)$$

where $\mathbf{u}^*$ is the shear velocity of the liquid, Sc is the Schmidt number and $\boldsymbol{\tau}_p^+$ is the dimensionless relaxation time of the inclusion. First term of the right hand side of equation 53 represents the Brownian effects, and the second term represents the inertial effects. [21]

3.3.4. 0-D model

0-D model is basically a homogeneous ladle system approach. Ladle is assumed to be perfectly agitated, so that parameters are considered constant within the bath. Macroscopic transport of inclusions is not considered due to the assumption of homogeneous system. Parameters are volume averaged over the volume of the ladle of the 3-D CFD case. Volume averaged quantities are: gas hold up, the bubble size and velocity, the sliding velocity, the turbulent kinetic energy, and its dissipation rate.

Equation 41 is transformed into equation

$$\frac{\partial N_i}{\partial t} = (\mathrm{B_i} - \mathrm{D_i}) - Z_{bi} - S_i - C_i, \qquad (54)$$

where C_i is the surface capture contribution. Equation 54 is solved by integrating over the volume of the reactor (V_r). 0-D modeling is used to reduce the calculation effort. [20]

Bellot et al. derived agglomeration and flotation models straight from the numerical heterogeneous model (3-D) so they are identical. Separation induced by gravity and the surface capture contribution have to be computed on the size of the entire reactor of height. [20]

Separation induced by gravity can be calculated with equation

$$S_i = \frac{u_s N_i}{H}, \qquad (55)$$

where H is the height of the entire reactor. [20]

Surface capture contribution can be calculated with equation

$$C_i = \frac{\boldsymbol{u}_{d,i} N_i}{H}. \text{ [20]} \qquad (56)$$

0-D model approach greatly depends on how well hydrodynamic properties can be volume averaged inside the reactor. Right estimation of volume averaged turbulent dissipation rate is crucial in order to have an accurate model. Because turbulent dissipation rate affects the agglomeration and flotation by their frequencies it is highly important parameter in 0-D model. [20]

Estimation of the collision frequency which Bellot et al. used is presented below. They consider for the sake of simplicity the Saffman and Turner model. The collision frequency β_{ij} for two given classes i and j only depends on the square root of the turbulent dissipation rate, which is shown below in equations 57[20] to 59[20].

$$\beta_{ij} = \beta_{ij}^{Stokes} + \beta_{ij}^{Turbulent} \qquad (57)$$

Stokes collision frequency is calculated with equation

$$\beta_{ij}^{Stokes} = \frac{2\pi g \left|\rho_l - \rho_p\right|}{9\mu_l} \left(\frac{d_{p,i} + d_{p,j}}{2}\right)^2 \left(\frac{d_{p,i}^2}{2} - \frac{d_{p,j}^2}{2}\right). \qquad (58)$$

Turbulent collision frequency is calculated with equation

$$\beta_{ij}^{Turbulent} = \sqrt{\frac{8\pi}{5}} \left(\frac{d_{p,i} + d_{p,j}}{2}\right)^3 \left(\frac{\varepsilon}{\nu}\right)^{0.5} \rightarrow \beta_{ij}^{Turbulent} \sim d_{i,j} \varepsilon^{0.5}. \qquad (59)$$

Turbulent collision frequency for given classes i and j only depends on square root of turbulent dissipation rate. [20]

Estimation of volume average of turbulent dissipation rate is calculated with equation

$$\bar{\varepsilon}^* = \left(\overline{\varepsilon^{\frac{1}{2}}}\right)^2 = \left(\frac{\int \varepsilon^{\frac{1}{2}} dv}{V_R}\right)^2. \text{ [20]} \qquad (60)$$

Estimation is used in order to minimize error in the calculation. Error comes from the difference between the average value of the collision frequency over the ladle and estimation of the collision frequency via mean value of turbulent dissipation rate shown in equation

$$\int \beta_{i,j}(\varepsilon)dv - \beta_{i,j}(\bar{\varepsilon})V_R = error.\ ^{[20]} \qquad (61)$$

3.3.5. Results and discussion

Bellot et al. tested and compared the models. Inclusion numeral density after 300 s is showed in Figure 11.

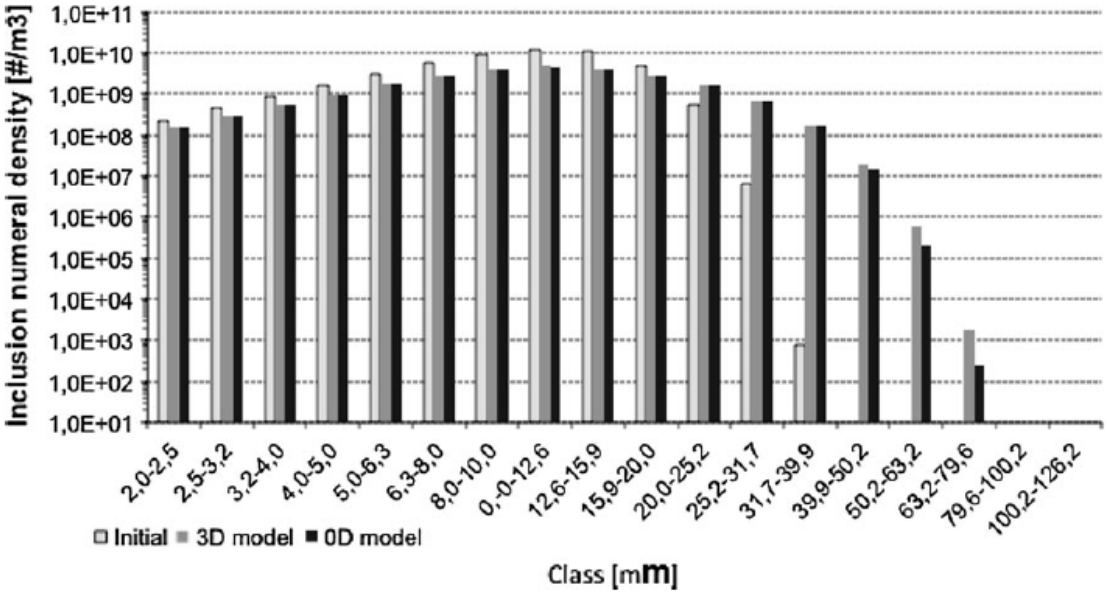

Figure 11. Inclusion numeral density as a function of size class after 300 s. [20]

In the Figure 11 it can be seen that the in the smaller inclusions agglomerate into larger inclusions and the number of small inclusions decreases when number of larger inclusions increases. 0-D (black) and 3-D (grey) models predict the amount of small inclusions well but the difference is seen in the case of large inclusions. The reason is seen in Figure 12. [20]

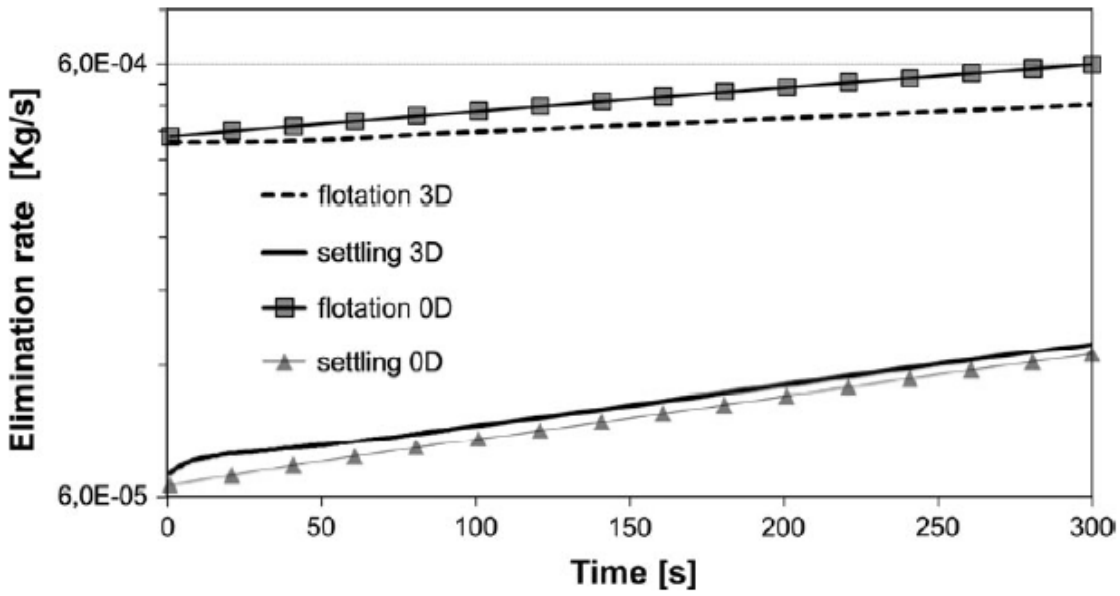

Figure 12. Elimination rate as a function of time. [20]

The Figure 12 tells that the 0-D model overestimates the flotation rate and underestimates the settling rate which gives rise to the error in the number of large inclusions (in comparison to the 3-D model). [20]

Bellot et al. showed that the total mass of inclusions remaining in the ladle over time and the Sauter's diameter for both models are in agreement. This means that 0-D model is very efficient approach to model the total number of inclusions in the ladle. Bellot et al. say that the 0-D model reduces the calculation effort a lot and it provides excellent prediction of the particle size distribution with process time. [20]

4. An in-house coupled-reaction model for estimating variations of slag/steel composition during ladle treatment

Simple module to calculate slag – steel composition changes during ladle treatment is presented in this chapter. The model was done at Aalto University by the author together with Dr. Shao Lei.

4.1. Calculating interfacial concentrations

In this module only interfacial reactions or separation of inclusions are considered and how they affect the composition of the steel and the slag and vice versa. CO formation and desulfurization are neglected.

Following reactions, equation

$$Fe + [O] = (FeO) \tag{62}$$

and

$$x[M] + y[O] = \left(M_x O_y\right) \tag{63}$$

are considered.

In this paper only silicon oxidation is considered for demo case.

Silicon oxidation reaction equation is

$$[Si] + 2[O] = (SiO_2). \tag{64}$$

Equilibrium constants K_{FeO} and K_{SiO2} for reactions above are calculated with equation

$$\log K_{FeO} = \frac{6372}{T} - 2.73 \tag{65}$$

and

$$\log K_{SiO_2} = \frac{31040}{T} - 12.\ ^{[26]} \tag{66}$$

At equilibrium equation

$$K_{FeO} = \frac{\gamma_{FeO} x_{FeO,I}}{f_O w_{O_I}} \tag{67}$$

and

$$K_{SiO_2} = \frac{\gamma_{SiO_2} x_{SiO_2,I}}{\left(f_O w_{O_I}\right)^2 f_{Si} w_{Si_I}} \tag{68}$$

are valid, where γ_i is the activity coefficient of substance i with respect to pure substance as standard state, f_i is the Henrian activity coefficient of element i, x_i is the mole fraction of substance i and w_i is the mass fraction of substance i in weight percent.

Mole fraction of slag components to mass fractions can be calculated using equation

$$x_i = \frac{\rho_s}{100 S_s} \frac{1}{M_i} w_i = B_i w_i \tag{69}$$

where S_s is the total molar concentration in slag (mol/m^3).

Equations 67 and 68 can be then noted as:

$$w_{FeO,I} = \frac{K_{FeO} f_O w_{O_I}}{\gamma_{FeO} B_{FeO,I}} \tag{70}$$

and

$$w_{SiO_2,I} = \frac{K_{SiO_2} \left(f_O w_{O_I}\right)^2 f_{Si} w_{Si_I}}{\gamma_{SiO_2} B_{SiO_2,I}} \tag{71}$$

Combining variables, equation

$$F_{FeO,I} = \frac{K_{FeO} f_O}{\gamma_{FeO} B_{FeO,I}} \tag{72}$$

and

$$F_{SiO_2,I} = \frac{K_{SiO_2} f_O^2 f_{Si}}{\gamma_{SiO_2} B_{SiO_2,I}} \tag{73}$$

can be obtained. And equations 70 and 71 are simplified into:

$$w_{FeO,I} = w_{O_I} F_{FeO,I} \tag{74}$$

and

$$w_{SiO_2,I} = w_{O_I}^2 w_{Si_I} F_{SiO_2,I} \quad (75)$$

Flux densities for substances are

$$J_O = k_m(n_{O,b} - n_{O,I}), \quad (76)$$

$$J_{FeO} = k_s(n_{Feo,I} - n_{Feo,b}), \quad (77)$$

$$J_{Si} = k_m(n_{Si,b} - n_{Si,I}) \quad (78)$$

and

$$J_{SiO_2} = k_s(n_{SiO_2,I} - n_{SiO_2,b}), \quad (79)$$

where n is the molar concentration (mol/m^3).

At equilibrium equation

$$J_{SiO_2} = J_{Si} \quad (80)$$

is true.

The amount of silicon out of the liquid steel is the same as the amount of silicon in the silicon oxide into the slag due to oxidation reaction. With this information equation

$$k_m(n_{Si,b} - n_{Si,I}) - k_s(n_{SiO_2,I} - n_{SiO_2,b}) = 0 \quad (81)$$

can be made.

Flux density of the oxygen into the interface from steel must be the same as flux density of the oxygen out of the interface to the slag. Oxygen is only found in oxides in the slag, in this example in SiO_2 and FeO. Flux density of oxygen out of the interface into the slag is the sum of all the fluxes that contain oxygen times the number of oxygen atoms in the compound. So for example in case of SiO_2: flux that contains oxygen is J_{SiO2}, and the number of oxygen atoms is 2. From the flux densities equation

$$J_O = 2J_{SiO_2} + J_{FeO} \quad (82)$$

is made.

As mentioned earlier at stationary state $J_{Si} = J_{SiO_2}$ is true, so it does not matter which notation is used. For simplicity J_{Si} is used.

So from the condition of electro-neutrality, one can obtain the following relation, combining equations 80 and 82.

$$2J_{Si} + J_{FeO} - J_O = 0 \tag{83}$$

Combining equations 76 to 78 and 83 equation

$$2k_m\left(n_{Si,b} - n_{Si,I}\right) + k_s\left(n_{Feo,I} - n_{Feo,b}\right) - k_m\left(n_{O,b} - n_{O,I}\right) = 0 \tag{84}$$

can be made.

Molar concentrations in equations 81 and 84 can be converted into mass fractions with equation

$$n_i = \frac{\rho_b}{100M_i} w_i. \tag{85}$$

Combining mass transfer coefficients into single parameter equation

$$\frac{k_m}{k_s} = k_{ratio} \tag{86}$$

is obtained. In the study of Kitamura et al. [27], they suggested based on experiments and industrial observations ratio of around 10.

Densities can be gathered also to a single constant:

$$\frac{\rho_s}{\rho_m} = \rho_{ratio}. \tag{87}$$

These can be only done if it is assumed that the densities and mass transfer coefficients do not vary with time.

Using equations 85 to 87 equations 83 and 84 can be transformed into the following equations:

$$\frac{1}{M_{Si}}\left(w_{Si,b} - w_{Si,I}\right) - \frac{\rho_{ratio}}{k_{ratio}}\frac{1}{M_{SiO2}}\left(w_{SiO_2,I} - w_{SiO_2,b}\right) = 0 \tag{88}$$

and

$$\frac{2}{M_{Si}}\left(w_{Si,b}-w_{Si,I}\right)+\frac{\rho_{ratio}}{k_{ratio}}\frac{1}{M_{FeO}}\left(w_{Feo,I}-w_{Feo,b}\right)-\frac{1}{M_O}\left(w_{O,b}-w_{O,I}\right)=0. \quad (89)$$

Above equations can be solved as they are independent and only have two unknown variables, e.g., $w_{Si,I}$ and $w_{O,I}$. $w_{Feo,I}$ and $w_{SiO_2,I}$ can be calculated with equations 74 and 75.

The Henrian activity coefficients (f_i) can be calculated, e.g., with Wagner's formalism, although the interaction parameters should be searched from literature.

The activity coefficients with respect to pure substance as standard state (γ_i) can be calculated by utilizing thermodynamics software or by the regression expressions presented in ref [28].

4.2. Variations of liquid steel – slag composition during ladle treatment

After all the interfacial concentrations are known, rate of change of bulk concentrations can be calculated. Rate of change of bulk mass fraction of silicon is shown as an example in equation

$$\frac{dw_{Si,b}}{dt}=-\frac{k_m A_I}{V_m}\left(w_{Si,b}-w_{Si,I}\right). \quad (90)$$

After discretizing the above equation and doing the same for all relevant substances equations

$$\frac{\Delta w_{Si,b}}{\Delta t}=\frac{w_{Si,b}|_{t+\Delta t}-w_{Si,b}|_t}{\Delta t}=-\frac{k_m A_I}{V_m}\left(w_{Si,b}|_t-w_{Si,I}|_t\right), \quad (91)$$

$$\frac{\Delta w_{O,b}}{\Delta t}=\frac{w_{O,b}\big|_{t+\Delta t}-w_{O,b}\big|_t}{\Delta t}=-\frac{k_m A_I}{V_m}\left(w_{O,b}\big|_t-w_{O,I}\big|_t\right), \quad (92)$$

$$\frac{\Delta w_{FeO,b}}{\Delta t}=\frac{w_{FeO,b}\big|_{t+\Delta t}-w_{FeO,b}\big|_t}{\Delta t}=\frac{k_s A_I}{V_s}\left(w_{FeO,I}\big|_t-w_{FeO,b}\big|_t\right) \quad (93)$$

and

$$\frac{\Delta w_{SiO_2,b}}{\Delta t} = \frac{w_{SiO_2,b}\big|_{t+\Delta t} - w_{SiO_2,b}\big|_t}{\Delta t} = \frac{k_s A_I}{V_s}\left(w_{SiO_2,I}\big|_t - w_{SiO_2,b}\big|_t\right) \qquad (94)$$

can be obtained. Mass transfer coefficients (k_m and k_s) and interfacial area (A_I) are needed to calculate above equations. Interfacial area is non-trivial to obtain. One method to avoid and go around the calculation of interfacial area is presented below. It can also be assumed that the interfacial area is the same as the area of the bath, but this leads to calculation error, because interfacial area is not flat and especially the stirring of the steel raises the interfacial area due to flow of steel. If the interfacial area is known or is calculated somehow following method is unnecessary and equations 91 to 94 can be used.

Volumetric mass transfer coefficients can be calculated with equation

$$\kappa_m = k_m A_I = \varphi_m V_m, \qquad (95)$$

where κ is the volumetric mass transfer coefficient (m^3/s) and φ is the auxiliary variable (1/s).

Auxiliary variable φ can be calculated with equations

$$\varphi_m = \frac{k_m A_I}{V_m} \qquad (96)$$

and

$$\varphi_m = \begin{cases} 0.013\dot{\varepsilon}^{0.25}, & \dot{\varepsilon} < 60W/t \\ 8.1 * 10^{-6}\dot{\varepsilon}^{2.1}, & \dot{\varepsilon} \geq 60W/t \end{cases}. \quad [1] \qquad (97)$$

It is noted that equation 101 is an empirical correlation.

Stirring power can be calculated, e.g., with equations 9 and equation

$$\dot{\varepsilon} = 14.23\left(\frac{QT_m}{W_m}\right)\log\left(\frac{1+h_v}{1.48P_0}\right), \qquad (98)$$

where P_0 is the gas pressure at the surface (atm).

Relation of volumetric mass transfer coefficients of liquid steel and slag:

$$\frac{\kappa_m}{\kappa_s} = \frac{k_m A_I}{k_s A_I} = \frac{k_m}{k_s} = k_{ratio} \tag{99}$$

Combining equations 96 and 99 equation

$$\kappa_s = \frac{\varphi_m V_m}{k_{ratio}} \tag{100}$$

can be obtained.

Using equation 100, equation

$$\varphi_s = \frac{k_s A_I}{V_s} = \frac{\varphi_m V_m}{V_s k_{ratio}} \tag{101}$$

can be obtained.

If volumes of liquid steel and slag are assumed to be constants (or close enough to constants) then equation

$$V_{ratio} = \frac{V_m}{V_s} \tag{102}$$

can be used.

If the auxiliary variable φ is used and stirring power is calculated with some equation, e.g. with equation 98, equations 91 to 94 can be converted into equations

$$\frac{\Delta w_{Si,b}}{\Delta t} = \frac{w_{Si,b}|_{t+\Delta t} w_{Si,b}|_t}{\Delta t} = -\varphi_m \left(w_{Si,b}|_t - w_{Si,I}|_t\right), \tag{103}$$

$$\frac{\Delta w_{O,b}}{\Delta t} = \frac{w_{O,b}\big|_{t+\Delta t} - w_{O,b}\big|_t}{\Delta t} = -\varphi_m \left(w_{O,b}\big|_t - w_{O,I}\big|_t\right), \tag{104}$$

$$\frac{\Delta w_{FeO,b}}{\Delta t} = \frac{w_{FeO,b}\big|_{t+\Delta t} - w_{FeO,b}\big|_t}{\Delta t} = \frac{\varphi_m V_{ratio}}{k_{ratio}} \left(w_{FeO,I}\big|_t - w_{FeO,b}\big|_t\right) \tag{105}$$

and

$$\frac{\Delta w_{SiO_2,b}}{\Delta t} = \frac{w_{SiO_2,b}\big|_{t+\Delta t} - w_{SiO_2,b}\big|_t}{\Delta t} \tag{106}$$

$$= \frac{\varphi_m V_{ratio}}{k_{ratio}} \left(w_{SiO_2,I}\big|_t - w_{SiO_2,b}\big|_t \right).$$

In the following section contents of Si and SiO_2 in the bulk phase and at the interface are illustrated as a function of time. The purpose is to show how the changes in different parameters affect the calculation. In the figures below bulk concentration of Si means the Si_b, which is the Si content in w-% in the liquid steel phase. At the interface Si content in w-% is Si_I. In the SiO_2 content in w-% figures bulk means the $SiO_{2,b}$, SiO_2 content in w-% in the slag phase. At the interface SiO_2 content in w-% is $SiO_{2,I}$

Table 5. Original values of the parameters used in the calculation of coupled-reaction model.

Parameter	Value	Unit
$F_{FeO,I}$	500	
$F_{SiO2,I}$	10^8	
$w_{Si_b,t=0}$	0.1	w-%
$w_{O_b,t=0}$	0.01	w-%
$w_{FeO_b,t=0}$	5	w-%
$w_{SiO_{2b},t=0}$	10	w-%
k_{ratio}	10	
κ_m	0.1	m^3/s
V_m	15	m^3
V_s	3	m^3
ρ_{ratio}	3/7	
Δt	1	s

The changes in the parameters are in each figure between 0.5 times and 1.5 times the original value of the parameter. The calculations were made with ten linearly spaced values of the parameter. In each figure lightest color represents the smallest value and darkest color represents the biggest value. Color is changing linearly from light to dark in each figure.

Figure 13 and Figure 14 are calculated with different values of the parameter k_{ratio}.

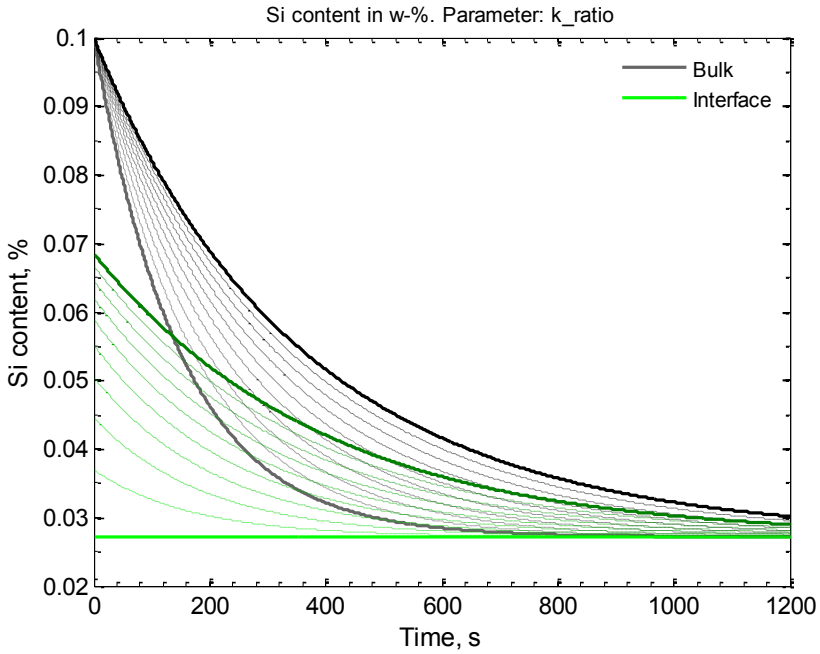

Figure 13. Si content in w-% as a function of time. Parameter in question is k_{ratio}. Lighter color represents smaller value and darker color represents bigger value of k_{ratio}.

It can be seen from the Figure 13 that when k_{ratio} decreases the Si content in liquid steel as well as the Si content in the interface decreases faster than when the k_{ratio} is increased. Also the final content of the Si in the liquid steel as well as in the interface is lower when k_{ratio} decreases.

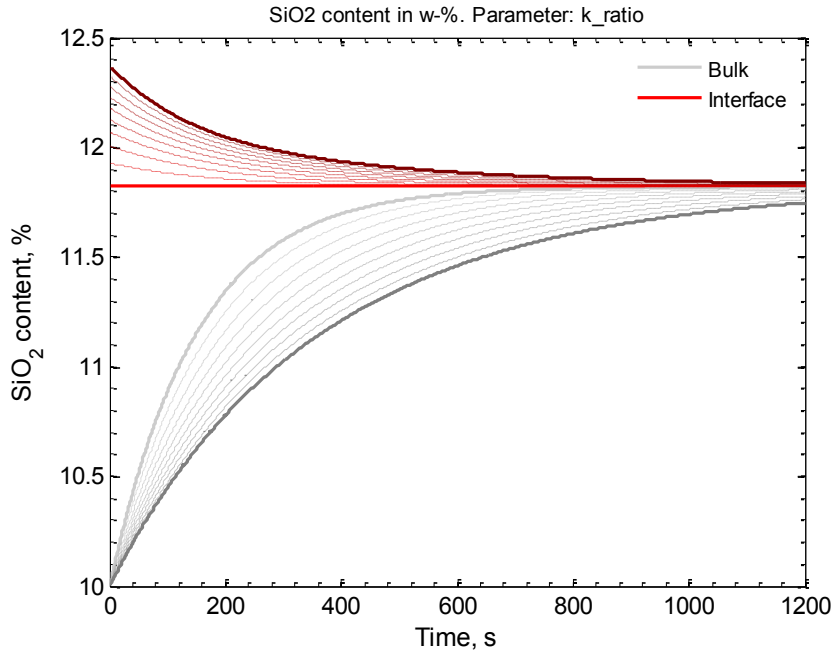

Figure 14. SiO_2 content in w-% as a function of time. Parameter in question is k_{ratio}. Lighter color represents smaller value and darker color represents bigger value of k_{ratio}.

From Figure 14 it can be seen that when the k_{ratio} is decreased SiO_2 content in the slag increases faster than when k_{ratio} is increased. When the k_{ratio} is decreased SiO_2 content in the interface decreases faster than when k_{ratio} is increased. Final content of SiO_2 in the slag is increased when k_{ratio} decreases.

Figure 15 and Figure 16 are calculated with different values of the parameter $F_{FeO,I}$.

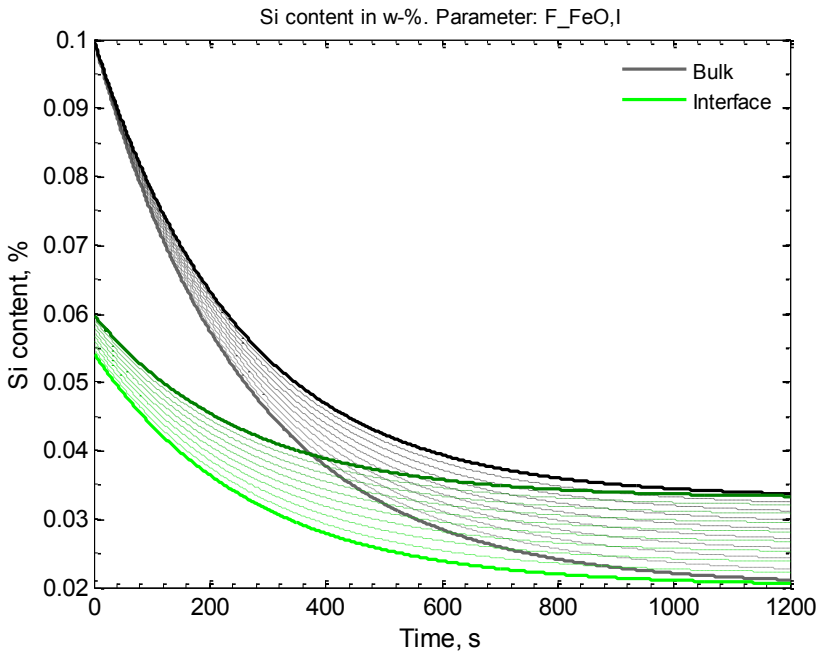

Figure 15. Si content in w-% as a function of time. Parameter in question is $F_{FeO,I}$. Lighter color represents smaller value and darker color represents bigger value of $F_{FeO,I}$.

It can be seen from the Figure 15 that when $F_{FeO,I}$ decreases the Si content in liquid steel as well as the Si content in the interface decreases faster than when the $F_{FeO,I}$ is increased. Also the final content of the Si in the liquid steel as well as in the interface is lower when $F_{FeO,I}$ decreases.

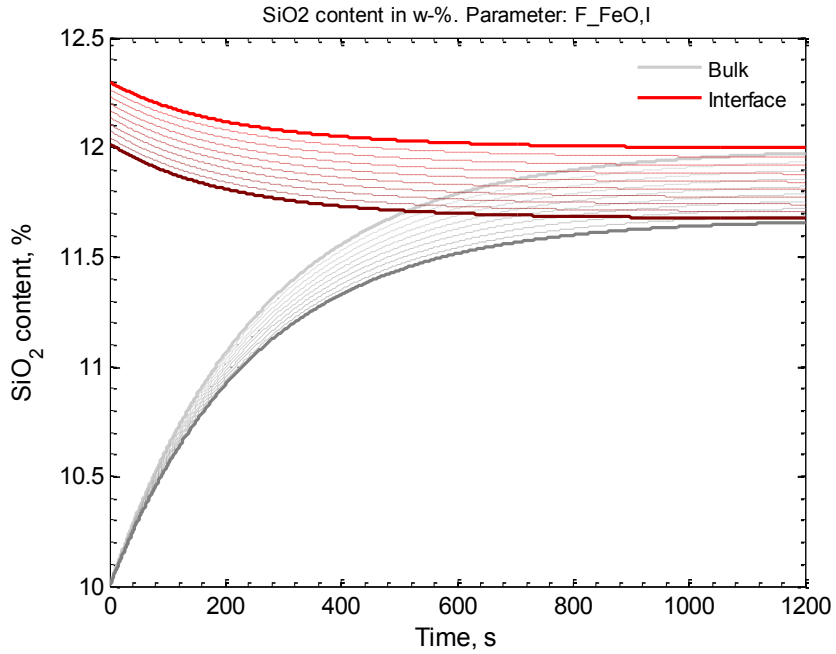

Figure 16. SiO_2 content in w-% as a function of time. Parameter in question is $F_{FeO,I}$. Lighter color represents smaller value and darker color represents bigger value of $F_{FeO,I}$.

From Figure 16 it can be seen that when the $F_{FeO,I}$ is decreased SiO_2 content in the slag increases faster than when $F_{FeO,I}$ is increased. Final content of SiO_2 in the slag as well as in the interface is increased when $F_{FeO,I}$ decreases.

Figure 17 and Figure 18 are calculated with different values of the parameter $F_{SiO2,I}$.

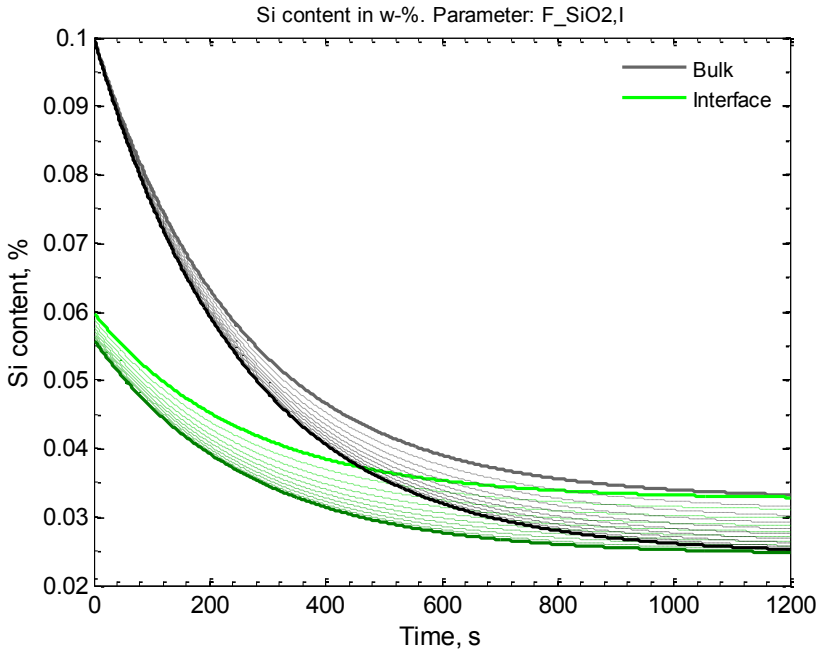

Figure 17. Si content in w-% as a function of time. Parameter in question is $F_{SiO2,I}$. Lighter color represents smaller value and darker color represents bigger value of $F_{SiO2,I}$.

It can be seen from the Figure 17 that when $F_{SiO2,I}$ increases the Si content in liquid steel as well as the Si content in the interface decreases faster than when the $F_{FeO,I}$ is decreased. Also the final content of the Si in the liquid steel as well as in the interface is lower when $F_{FeO,I}$ increases.

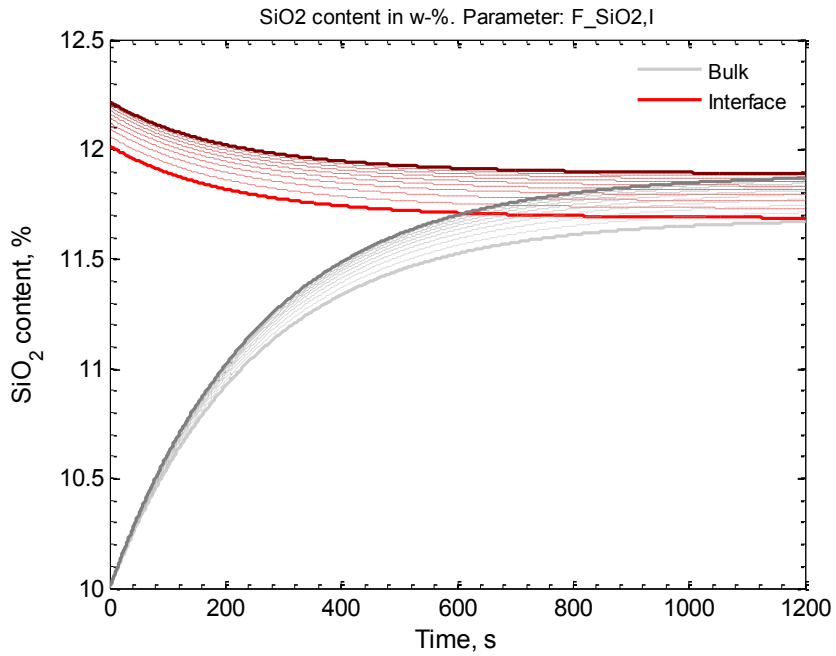

Figure 18. SiO_2 content in w-% as a function of time. Parameter in question is $F_{SiO2,I}$. Lighter color represents smaller value and darker color represents bigger value of $F_{SiO2,I}$.

From Figure 18 it can be seen that when the $F_{SiO2,I}$ is decreased SiO_2 content in the slag increases slower than when $F_{SiO2,I}$ is increased. Final content of SiO_2 in the slag as well as in the interface is increased when $F_{SiO2,I}$ increases.

Figure 19 and Figure 20 are calculated with different values of the parameter $FeO_{b,t=0}$.

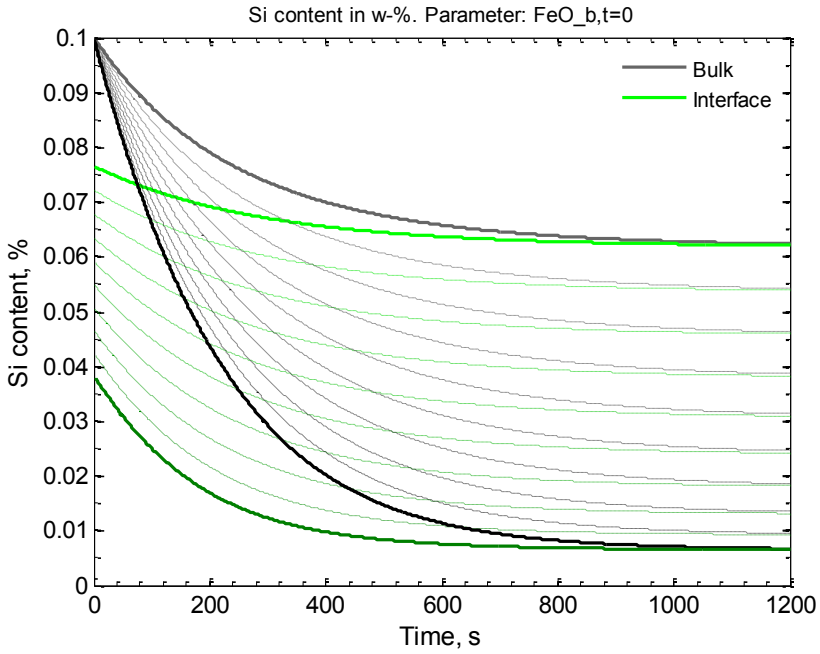

Figure 19. Si content in w-% as a function of time. Parameter in question is $FeO_{b,t=0}$. Lighter color represents smaller value and darker color represents bigger value of $FeO_{b,t=0}$.

It can be seen from the Figure 19 that when $FeO_{b,t=0}$ increases the Si content in liquid steel as well as the Si content in the interface decreases faster than when the $FeO_{b,t=0}$ is decreased. Also the final content of the Si in the liquid steel as well as in the interface is lower when $FeO_{b,t=0}$ increases.

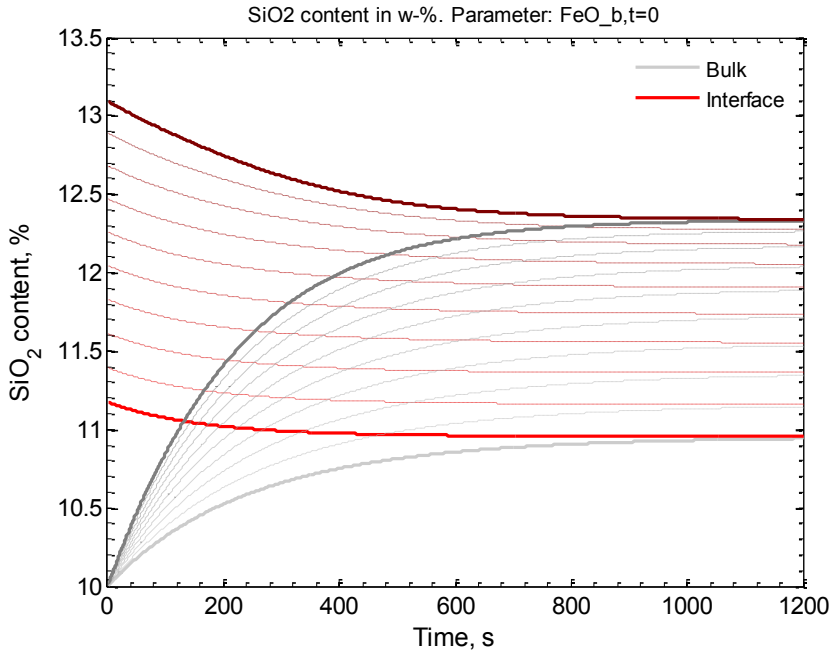

Figure 20. SiO_2 content in w-% as a function of time. Parameter in question is $FeO_{b,t=0}$. Lighter color represents smaller value and darker color represents bigger value of $FeO_{b,t=0}$.

From Figure 20 it can be seen that when the $FeO_{b,t=0}$ is decreased SiO_2 content in the slag increases slower than when $FeO_{b,t=0}$ is increased. Final content of SiO_2 in the slag as well as in the interface is increased when $FeO_{b,t=0}$ increases.

Figure 21 and Figure 22 are calculated with different values of the parameter $Si_{b,t=0}$.

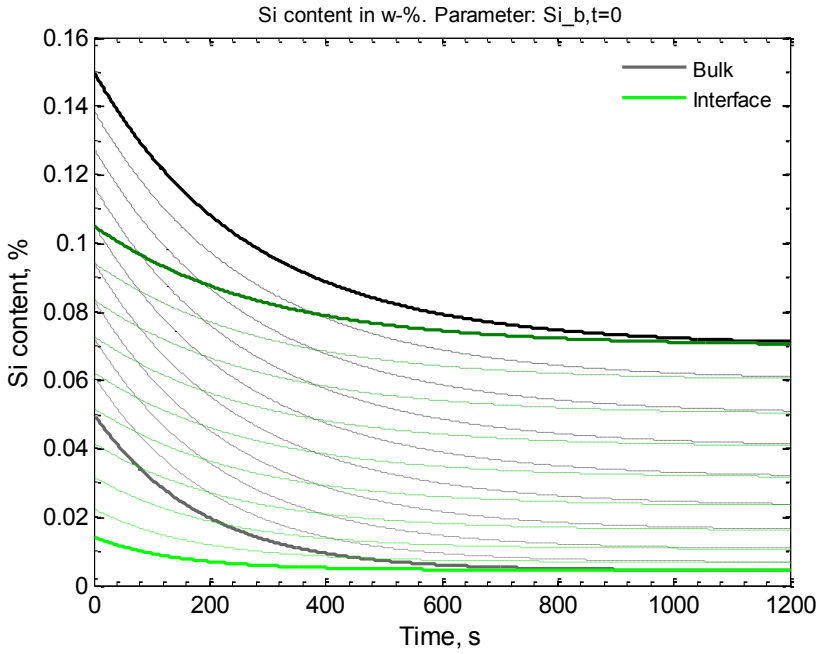

Figure 21. Si content in w-% as a function of time. Parameter in question is $Si_{b,t=0}$. Lighter color represents smaller value and darker color represents bigger value of $Si_{b,t=0}$.

It can be seen from the Figure 21 that when $Si_{b,t=0}$ decreases the final Si content in liquid steel as well as the Si content in the interface decreases.

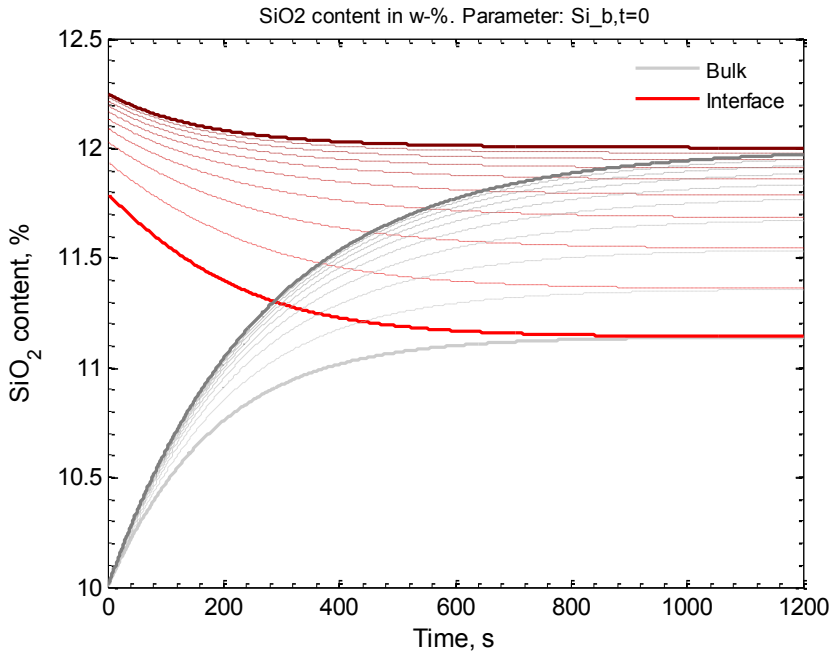

Figure 22. SiO_2 content in w-% as a function of time. Parameter in question is $Si_{b,t=0}$. Lighter color represents smaller value and darker color represents bigger value of $Si_{b,t=0}$.

From Figure 22 it can be seen that when the $Si_{b,t=0}$ is decreased SiO_2 content in the slag increases slower than when $Si_{b,t=0}$ is increased. Final content of SiO_2 in the slag as well as in the interface is increased when $Si_{b,t=0}$ increases.

Figure 23 and Figure 24 are calculated with different values of the parameter $SiO_{2,b,t=0}$.

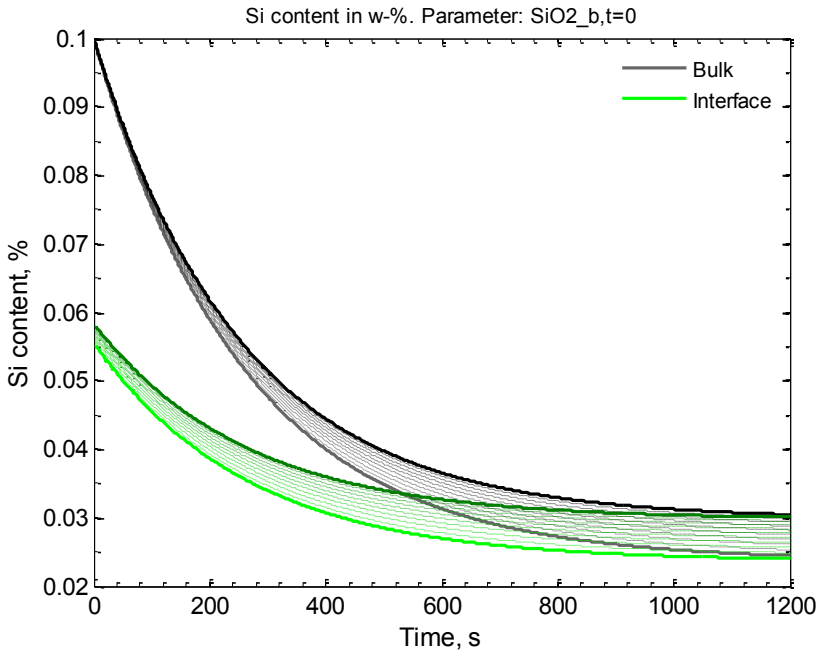

Figure 23. Si content in w-% as a function of time. Parameter in question is $SiO_{2,b,t=0}$. Lighter color represents smaller value and darker color represents bigger value of $SiO_{2,b,t=0}$.

It can be seen from the Figure 23 that when $Si_{b,t=0}$ decreases the Si content in liquid steel as well as the Si content in the interface decreases faster than when the $Si_{b,t=0}$ is decreased. Also the final content of the Si in the liquid steel as well as in the interface is lower when $Si_{b,t=0}$ decreases.

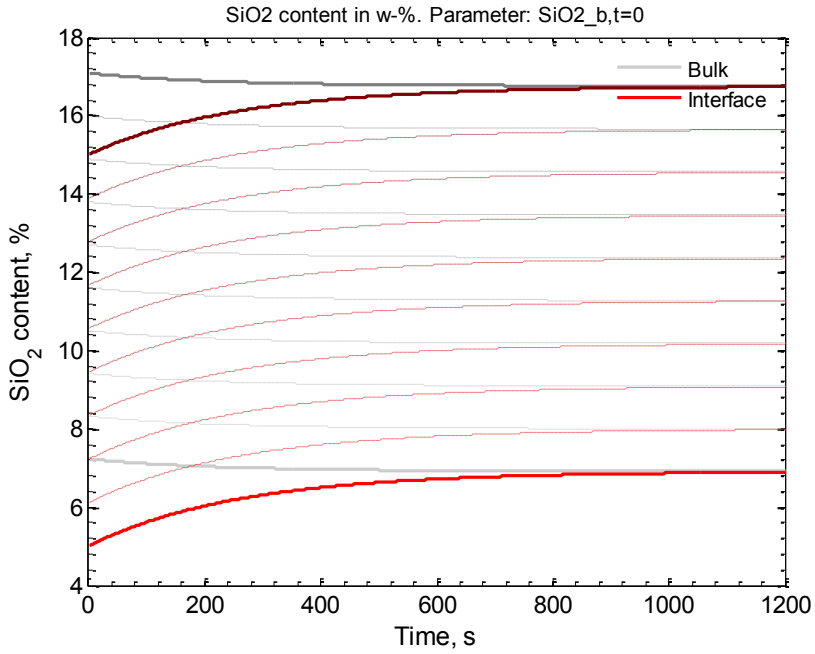

Figure 24. SiO_2 content in w-% as a function of time. Parameter in question is $SiO_{2,b,t=0}$. Lighter color represents smaller value and darker color represents bigger value of $SiO_{2,b,t=0}$.

From Figure 24 it can be seen that when $SiO2_{b,t=0}$ increases the final SiO_2 content in the slag as well as the Si content in the interface increases.

In Table 6 the observations from the Figure 13 to Figure 24 are collected. The removal of Si is showed as compared to the original value of the parameters. Arrows in Table 6 represent does the removal of Si get better (↑) or worse (↓) when parameter is decreased.

Table 6. The change of removal of Si when the parameter is smaller than the original value is presented. The opposite change happens when the parameter value of higher than the original value. The upward arrow corresponds better removal of Si and the downward arrow corresponds worse removal of Si compared to the original removal of Si.

	Removal of Si
k_{ratio}	↑
$F_{FeO,\,l}$	↑
$F_{SiO2,\,l}$	↓
$w_{FeO_b,t=0}$	↓
$w_{Si_b,t=0}$	↑
$w_{SiO_{2b},t=0}$	↑

5. Discussion

In this chapter models from the literature and the experimental part of this work are discussed. The purpose of this work is to present different models, ideas and methods for calculating online the composition, amount and size of inclusions in the liquid steel. The model must be fast (calculation effort small) but accurate (the model must predict the inclusion evolution correct enough). These two main points must be kept in mind at all times.

Harada et al. does not model transiently the mixing in the ladle. They just calculate the perfect mixing time. The perfect mixing time calculation is fast (analytical equation) but transient solution is not obtained. Bellot et al. on the other hand solves the flow field of the steel melt using CFD but the calculations are slow. Shu & Scheller modeled the mixing with tanks in series method. The method is faster but less accurate than the CFD approach. On the calculation effort side it is also on the middle of the three models. The CFD model of Bellot et al. is too complex and slow to be good method for online modeling. Perfect mixing time calculation also might not be suitable. Transient solution is better in the way that it is more versatile. Therefore tanks in series method is promising method for online modeling.

Reactions between liquid steel and slag were modeled by Harada et al. with coupled reaction model. Reactions are described with double film theory. At the interface equilibrium conditions are assumed. Bellot et al. do not show how they modeled the liquid steel – slag interaction. They consider entrapment of slag into the liquid steel. Shu & Scheller modeled the liquid steel – slag interaction with equilibrium calculation. They assumed that small part of liquid steel and slag react with each other near the interface and they calculated with equilibrium calculation how the phases react at the interface.

Both models by Harada et al. as well as Shu & Scheller are promising and both methods should be researched more for online use.

Inclusions originating from the slag are the inclusions resulting from the entrapment of top slag in the liquid steel. Harada et al. assumed that the volume ratio between slag and the entrapment of slag into the liquid steel is constant. Therefore Harada et al. assumed that the entrapment of inclusion originating from slag is constant. Shu & Scheller did not model inclusions originating from slag calculations. Bellot et al. modeled the inclusions originating from slag with deposition law.

Harada et al. assumed that volume ratio of deoxidation products which agglomerates with inclusions originating from slag is constant. They also assumed that volume ratio of deoxidation products and inclusions originating from slag which floats into the slag is constant. Therefore Harada et al. assumed that the agglomeration and flotation rates are constant.

Bellot et al. modeled the agglomeration and flotation with PBE. They also modeled the separation induced by gravity. This is the most accurate of the presented models but also the most complex.

Shu & Scheller modeled the inclusions to flow together with the bulk phase. The separation of inclusions is calculated with separation percentages for inclusions. This means that in every time step separation percentage tells how much of the inclusions separate into the top slag.

All the models are interesting. The problem with model by Bellot et al. is that even the 0-D PBE calculation might be too slow and it requires flow field solution using CFD. The model by Shu & Scheller seems to be really simple and the accuracy is a question but their separation percentages are based on experimental results. Harada et al. modeled a lot with constant parameters and it should be researched how well the constant assumption models the phenomena. Without further knowledge it is recommended that all models should be researched more.

The model made by Bellot et al. is the only one where size distribution of the inclusions is calculated using population balance equations. 3-D PBE is possibly more accurate than the 0-D PBE but 0-D PBE gives reasonably good estimates and is a lot lighter than

the 3-D on calculation effort. The problem with the Bellot et al. model is that they do not take into account different inclusions (Al2O3, CaO, etc.). It is assumed that all the inclusions are the same or just general inclusion.

Size distribution of the inclusions is really important aspect of the quality of the steel. Therefore it is recommended that 0-D model of Bellot et al. should be researched more for offline model.

Harada et al. assumed that refractory dissolves into the slag but not into the liquid steel (very slow dissolution). Bellot et al. say that they modeled entrapment at the ladle walls but they do not show how they modeled it. Shu & Scheller assumed that there is a constant dissolution of refractory into the liquid steel as well as into the slag.

The methods done by Harada et al. and Shu & Scheller are promising and both methods are computationally fast. The constant dissolution rate assumption by Shu & Scheller yields a small error but the refractory dissolution is not the most crucial point of the online model. Therefore it is recommended to research both models by Harada et al. and Shu & Scheller more.

The coupled reaction model was presented as well as the sensitivity analysis of the coupled reaction model. The model should be compared to literature values but good comparison was not found. Sensitivity analysis was carried due to lack of literature comparison. Sensitivity analysis shows that the model is not sensitive to the range of values that were tested. The future development is then to find realistic estimations to the parameters in the model.

The faster the Si content in the liquid steel drops as low as possible the faster the removal of Si from the liquid steel. Also the faster the Si content in the interface drops as low as possible the faster the oxidation of silicon. From the Table 6 following things are noted. Removal of Si is faster when the values of k_{ratio}, $F_{FeO,I}$, $Si_{b,t=0}$, $SiO_{2b,t=0}$ are smaller than the original values. Removal of Si is faster when the values of $F_{SiO2,I}$ and $FeO_{b,t=0}$ are higher than the original values. It can be also seen from the Figure 13 to

Figure 24 that when the removal of the Si from the liquid steel is better than in the original situation the oxidation of silicon at the interface is also better.

6. Conclusion

Phenomena affecting the ladle process are numerous and all the relevant phenomena should be considered in the making of the online model. The calculation effort must be small in order to have an online model. Simplifying the phenomena for the model usually decreases the calculation effort. The problem lies in the accuracy: how much error the simplifying makes in the prediction of the inclusion population in the liquid steel.

The model made by Bellot et al. is the most complex of the three but the problem is the calculation time. Therefore it is not suitable candidate to the online model. 0-D PBE seems fascinating but the calculations might still be too slow. It remains a question does the 0-D model work at all if CFD calculations are replaced with simpler calculations (e.g. tanks in series) or if estimations of the parameters used in the 0-D model are used. This model is still useful for offline research because it can give estimates for the size distribution of the inclusions.

Harada et al. as well as Shu & Scheller made interesting models for calculating the steel/slag/inclusion compositions during the ladle process. Many things they have done can be incorporated into the online model. Tanks in series method that Shu & Scheller used is proposed as a basis of mixing module in the upcoming online model. Approaches for modeling refractory dissolution and inclusion modeling (transport, agglomeration, flotation, separation and entrapment) by Harada et al. as well as Shu & Scheller are recommended to be researched more.

Sensitivity analysis of the coupled reaction model was done and it showed that the model is not sensitive to the range of values that were tested. In future it is important to find realistic estimations to the parameters in the model and to further develop the model to take into account oxidation of all relevant elements.

References

[1] R. J. Fruehan, The Making Shaping and Treating of Steel, 1998, The AISE Steel Foundation, United States of America, ISBN: 0-930767-02-0

[2] Kasimagwa, I. A study on the behavior of the slag-line refractory during steel production. Doctoral thesis. (2014)

[3] Yi Chens. (2011) (Cited in Kasimagwa 2014), Numerical and Experimental Study of Marangoni Flow on the Slag-line Dissolution of Refractories, PhD Thesis, McMaster University, Hamilton, Ontario, Canada.

[4] K. Mukai. (1992). Wetting and Marangoni Effect in Iron and Steelmaking Processes. ISIJ International, Vol. 32, No. 1, pp 19-25.

[5] Holappa, L. (2013). Secondary Steelmaking. Treatise on Process Metallurgy, Volume 3: Industrial Processes, 3, 301.

[6] Kim, S. H., & Fruehan, R. J. (1987). Physical modeling of liquid/liquid mass transfer in gas stirred ladles. Metallurgical Transactions B, Vol. 18, No. 2. pp. 381-390.

[7] Brimacombe, J. K.; Cramb, A. W. Steel Refining Processes for Product Quality. In: Scaninject VI. 6 th International Conference on Refining Processes. I. 1992. p. 71-111.

[8] Colavito, D. M., Damiano, J., & Vermeulen, Y. C. (2012). U.S. Patent No. 8,221,677. Washington, DC: U.S. Patent and Trademark Office.

[9] http://www.steeluniversity.org/content/html/eng/default.asp?catid=100&pageid=240651470 Last accessed 5.8.2014.

[10] Harada, A., Maruoka, N., Shibata, H., & Kitamura, S. Y. (2013). A Kinetic Model to Predict the Compositions of Metal, Slag and Inclusions during Ladle Refining: Part 1. Basic Concept and Application. ISIJ international, Vol 53, No. 12. pp. 2110-2117.

[11] Harada, A., Maruoka, N., Shibata, H., & Kitamura, S. Y. (2013). A Kinetic Model to Predict the Compositions of Metal, Slag and Inclusions during Ladle Refining: Part2. Condition to Control the Inclusion Composition. ISIJ international, Vol. 53, No. 12. pp. 2118-2125.

[12] Lehrer, L. H. (1968). Gas agitation of liquids. Industrial & Engineering Chemistry Process Design and Development, Vol. 7, No. 2. pp. 226-239.

[13] Shu, Q., Scheller, P. Modification of inclusion composition in steel during secondary metallurgical ladle treatment.

[14] Scheller, P. R. and Shu, Q. (2014), Inclusion Development in Steel During Ladle Metallurgical Treatment - A Process Simulation Model – Part: Industrial Validation. steel research int., 85: 1310–1316. doi: 10.1002/srin.201300375

[15] Hongbin. Yin, H. Shibata, T. Emi, M. Suzuki. (1997). Characteristics of Agglomeration of Various Inclusion Particles on Molten Steel Surface. ISIJ International. Vol 37. No. 10, pp. 946-955.

[16] Kang, Y., Sahebkar, B., Scheller, P. R., & Sichen, D. (2007). Some aspects of physical growth of non-metallic inclusion in ladle treatment. METEC InSteelCon, Dusseldorf, Germany

[17] Y. J. Kang, B. Sahebkar, K. Morita, P. R. Scheller, D. Sichen. (2011). Observation on Phusical Growth of Nonmetallic Inclusion in Liquid Steel During Ladle Treatment. Metallurgical and Materials Transactions B, Vol 42, Issue 3. pp. 522-534.

[18] S. H. Lee, C. Tse, K.W. Yi, P. Misra, V. Chevrier, C. F. Orrling, S. Sridhar, A. W. Cramb,(2001). Separation and dissolution of Al2O3 inclusions at slag/metal interfaces. Journal of Non-Crystalline Solids. Vol 282, Issue 1. pp. 41-48. doi:10.1016/S0022-3093(01)00327-1.

[19] C. E. Grip, M. Yano, S. Kitamura, K. Harashima, K. Azuma, N. Ishiwata, Y. Obana, R. Marsh, F. Donahue, N. Takashiba, H. Okamoto, K. Aizawa, N. Bannenberg, H. Lachmund, B. Prothman, R. T. C. E. Adair, Chapter: Steelmaking II - Ladle metallurgy; 77th Steelmaking conference proceedings, Chicago, US, March 20–23, 1994, pp. 103–149.

[20] Bellot, J. P., De Felice, V., Dussoubs, B., Jardy, A., & Hans, S. (2014). Coupling of CFD and PBE Calculations to Simulate the Behavior of an Inclusion Population in a Gas-Stirring Ladle. Metallurgical and Materials Transactions B, Vol 45, No. 1. pp. 13-21.

[21] Felice, V. D., Daoud, I. L. A., Dussoubs, B., Jardy, A., & Bellot, J. P. (2012). Numerical modelling of inclusion behaviour in a gas-stirred ladle. ISIJ international, Vol 52, No. 7. pp. 1273-1280.

[22] Kumar, J., Peglow, M., Warnecke, G., Heinrich, S., & Mörl, L. (2006). Improved accuracy and convergence of discretized population balance for aggregation: The cell average technique. Chemical Engineering Science, Vol. 61, No. 10. pp. 3327-3342.

[23] Stanković I, Žeželj M, Belić A. Aggregation kinetics of short-range attractive particles: Brownian Dynamics simulations vs. Smoluchowski equation. Scientific Computing Laboratory, Institute of Physics Belgrade, University of Belgrade, Serbia. Visited last on 7.7.2015. http://www.scl.rs/papers/bdag.pdf

[24] Zaichik, L., Simonin, O., & Alipchenkov, V. (2010). Turbulent collision rates of arbitrary-density particles. International Journal of Heat and Mass Transfer, Vol. 53, No. 9. pp. 1613-1620.

[25] Xayasenh, A., Duval, H., & Joly, L. (2010). Qualitative analysis of inclusion turbulent deposition at liquid metal/slag interface.

[26] Deo, B., & Boom, R. (1993). Fundamentals of steelmaking metallurgy. Prentice-Hall. page 52

[27] Kitamura, S. Y., Kitamura, T., Shibata, K., Mizukami, Y., Mukawa, S., & Nakagawa, J. (1991). Effect of stirring energy, temperature and flux composition on hot metal dephosphorization kinetics. ISIJ international, Vol. 31, No. 11. pp. 1322-1328.

[28] Ohta H., Suito H. (1998). Activities of SiO_2 and Al_2O_3 and activity coefficients of Fe_tO and MnO in $CaO\text{-}SiO_2\text{-}Al_2O_3\text{-}MgO$ slags. Metallurgical and Materials Transactions B, Vol 29, Issue 1. pp. 119-129. DOI: 10.1007/s11663-998-0014-1.